

# Fast and Robust Certifiable Estimation of the Relative Pose Between Two Calibrated Cameras

Mercedes Garcia-Salguero\* and Javier Gonzalez-Jimenez†

Machine Perception and Intelligent Robotics (MAPIR) Group, System Engineering and Automation Department,  
University of Malaga, Campus de Teatinos, 29071 Malaga, Spain  
Email: \*mercedesgarsal@uma.es, †javiergonzalez@uma.es

**Abstract**—This work contributes an efficient algorithm to compute the Relative Pose problem (RPP) between calibrated cameras and certify the optimality of the solution, given a set of pair-wise feature correspondences affected by noise and probably corrupted by wrong matches. We propose a family of certifiers that is shown to increase the ratio of detected optimal solutions. This set of certifiers is incorporated into a fast essential matrix estimation pipeline that, given any initial guess for the RPP, refines it iteratively on the product space of 3D rotations and 2-sphere. In addition, this fast certifiable pipeline is integrated into a robust framework that combines Graduated Non-convexity and the Black-Rangarajan duality between robust functions and line processes.

We proved through extensive experiments on synthetic and real data that the proposed framework provides a fast and robust relative pose estimation. We make the code publicly available <https://github.com/mergarsal/FastCertRelPose.git>.

## I. INTRODUCTION

The Relative Pose problem (RPP) consists of finding the relative rotation  $\mathbf{R}$  and translation  $\mathbf{t}$  between two central, calibrated cameras given a set of  $N$  pair-wise feature correspondences  $(\mathbf{f}_i, \mathbf{f}'_i)$ , as shown in Figure (1). Since the scale cannot be recovered for this type of configurations, the translation component is estimated only *up-to-scale* [1].

Estimating the relative pose from visual data is the cornerstone of tasks such as visual odometry [2]–[4], and more complex computer vision problems *e.g.*, Simultaneous Localization and Mapping (SLAM) [5]–[7] and Structure-from-Motion (SfM) [8]–[10]. The gold-standard approach for RPP poses it as a 2-view Bundle Adjustment (BA) that minimizes the reprojection error [1], [11], [12]. This is a non-convex problem that typically presents multiple local minima. Since the algorithms employed for its resolution are iterative, they are prone to get stuck in suboptimal solutions, which may lay arbitrarily far away from the global minimum. The lack of quality of these solutions may hinder the subsequent blocks of the applications that leverage them, leading to inaccurate solutions or even to the complete failure of the application. An example of the last case is shown in Figure (2), where the left reconstruction employs all the solutions, while the right reconstruction *only* employed those solutions certified as global optima (we return to this certification later on this introduction). Therefore, special attention must be given to this fundamental and early block on these complex applications.

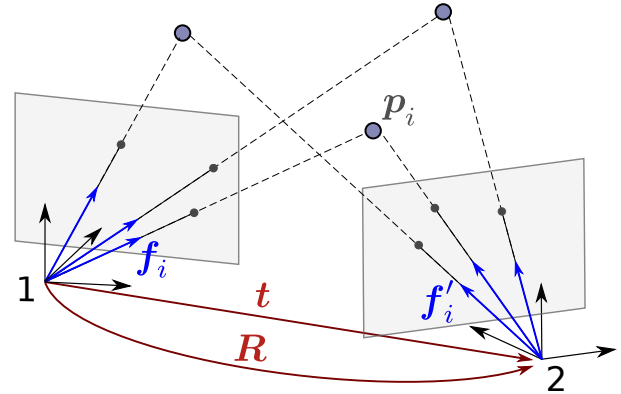


Fig. 1: The RPP seeks the relative pose, orientation  $\mathbf{R}$  and translation  $\mathbf{t}$  up-to-scale between two calibrated, central cameras given a set of  $N$  pair-wise feature correspondences. Figure from [13].

In order to try to avoid these suboptimal solutions for the RPP, a good initialization is usually required [14]. If this initial guess is within the attraction basin of the optimal solution, the iterative method will return it with high probability [11]. Although, in general, the quality of the initial guess cannot be measured, it has been reported in the literature that simplifications of the problem lead to good initializations. A common simplification for the RPP relies on the algebraic error and the so-called *essential matrix*  $\mathbf{E}$  [1], which is a  $3 \times 3$  matrix that encapsulates all the geometric information about the relative pose (rotation and translation) and it is defined as  $\mathbf{E} \doteq [\mathbf{t}]_{\times} \mathbf{R}$ , where  $[\mathbf{t}]_{\times}$  denotes the matrix form for the cross-product for a 3D vector such that  $\mathbf{t} \times \bullet = [\mathbf{t}]_{\times} \bullet$  (we define its explicit form later in Equation (1)).

The essential matrix constrains the pair-wise correspondences  $(\mathbf{f}_i, \mathbf{f}'_i)$  via the *epipolar constraint*, formally defined as  $\mathbf{f}_i^T \mathbf{E} \mathbf{f}'_i = 0$ . Here the observations  $\mathbf{f}_i, \mathbf{f}'_i$  are 3D vectors, which can be expressed in homogeneous coordinates (last entry to one) or normalized (Euclidean norm to one). While this relation holds for all the correspondences when they are noiseless, in real scenarios  $\mathbf{f}_i^T \mathbf{E} \mathbf{f}'_i = \epsilon_i$ , with  $\epsilon_i \neq 0$ , usually known as the *epipolar error*. A common approach leverages this relation in order to find the “best” essential matrix in terms of this error, *i.e.* we seek the  $\mathbf{E}$  that minimizes  $\epsilon_i^2$  for all the

correspondences,  $\sum_{i=1}^N \epsilon_i^2$  [1], [15]. Although more complex errors are employed in the literature, see for example [16], [17], this is already a complex, non-convex problem, hence presenting multiple local minima.

The relative pose, and hence the essential matrix, has five degrees of freedom, three for the 3D rotation, three for the 3D translation and one less due to the scale ambiguity. Since the epipolar constraint is linear in the entries of  $E$ , at least five correspondences are required to estimate it (except for degenerate cases [1], [18]). This is known as the minimal solver (the five-point algorithm, 5-PT) [19], [20]. This solver can be embedded into robust paradigms, such as RANSAC [21], [22], in order to gain robustness against wrong correspondences, *i.e.* outliers.

Although the 5-PT is the minimal solver for this problem, another common approach is the eight-point algorithm, 8-PT [1], [23], [24]. This method employs eight points, and although it was initially devised for the *fundamental matrix*, the equivalent version of the essential matrix for uncalibrated cameras, it can be adapted to the calibrated case in a straightforward manner. The main advantage of this solver is its simplicity, since the solution is obtained by first computing the Singular Value Decomposition of the data matrix (formed by the pair-wise correspondences) and then projecting the right singular vector associated with the smallest singular value onto the space of essential matrices [1], [24]. Further, this approach admits an extension that includes all the correspondences, known as the Direct Linear Transformation (DLT). However, the solution found by these methods is only the global optimum in theory when correspondences are noiseless [25]. These (suboptimal) solutions from the closed-form solvers are usually refined by

iterative algorithms that respect the intrinsic constraints of the essential matrices, see *e.g.* [13], [16], [26]. However, since the problem is still non-convex, these iterative algorithms may still return suboptimal solutions [14].

Some works have proposed certifiable solvers for the non-minimal RPP, that is, solvers that *guarantee* that the returned solution is the global optimum, among others [12], [15], [27]. They make use of off-the-shelf optimization tools that have polynomial or even exponential time complexity. Although fast implementations has been reported, see [15], they are still slow for the computer vision standards (30 fps). On the bright side, these solvers are not the only ones that are able to certify optimality. Banderia [28] characterized the so-called Certifiable Algorithms that, for a given solution to a non-convex problem (obtained by any means) and for most real-world problem instances, are able to certify if the solution is optimal, provided some conditions are fulfilled. Such certifiable algorithms have been reported previously in the literature for other problems, such as rotation averaging [29], point set registration [30], [31] or pose graph optimization [32]–[34]. The main advantage of these approaches is that they are usually faster in terms of certification than the above-mentioned certifiable proposals. Further, since the solution to the non-convex problem can be estimated by any iterative method, the estimation stage is also faster than the exponential tools, see *e.g.* [26]. In [13], we proposed for the first time this kind of certifiable algorithm for the RPP, which was demonstrated to be faster than the state-of-the-art solver under a MATLAB implementation.

Nevertheless, the above-mentioned approaches (with some exceptions, like [15]) do not consider explicitly the presence of bad correspondences (outliers), which strongly affect the accuracy of the solution. Outliers are common in real-world problem instances due to the nature of the feature detection algorithms and matching processes. The classic approach to detect these bad correspondences relies on the embedding of a minimal solver into a RANSAC framework [11], [22], [35]. The returned set of inliers is then employed to estimate the essential matrix by any of the previously mentioned methods. To overcome some of the limitations that such strategies present, attention has been recently directed to tools known as Graduated Non-convexity (GNC) [36] and the Black-Rangarajan (BR) [37] duality between robust estimations and line processes. In combination, they permit to estimate both the set of inliers and the solution to a given (non-convex) problem. The potential of these tools has been reported in, for example, [15], [38], [39], demonstrating to outperform RANSAC-based strategies in accuracy while being robust up to a higher percentage of outliers.

**Contributions:** In this work, we extend our proposal in [13] for the RPP with two significant improvements: a family of optimality certifiers and a robust paradigm for the non-minimal solver based on GNC and BR.

More precisely, the main technical contributions of the present work are:

- 1) We define in Section (V) the set of optimality certifiers

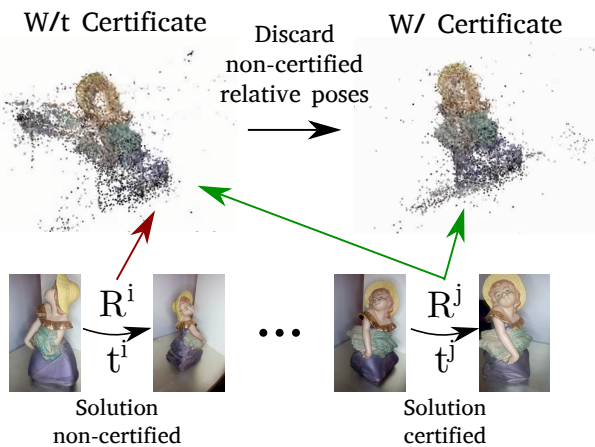


Fig. 2: Suboptimal solutions for the RPP may lead to inaccurate solutions or even the complete failure of those applications that employed the RPP as fundamental block. The left reconstruction (W/T CERTIFICATE) is performed with all the solutions for the RPP, while the right reconstruction (W/ CERTIFICATE) only employs those solutions certified as optimal. Some of the images employed for the reconstruction are included below.

associated with the different relaxations of the set of essential matrices. This family of certifiers is shown to detect (certify) more optimal solutions, overcoming in most problem instances the limitations associated with the different relaxations and their tightness.

- 2) We provide in Section (V-A) the quadratic Euclidean model of the RPP whose objective function is the squared, normalized epipolar error, defined over the product space of 3D rotation matrices and the 2-sphere. A preconditioner that decreases the convergence time of the iterative method is also provided.
- 3) We illustrate in Section (VI) the embedding of the RPP into the robust framework formed by the combination of GNC and BR, providing also a general library for its utilization (not restricted to the RPP) in <https://github.com/mergarsal/GNCSO.git>.
- 4) We perform extensive experiments in Section (VII) on both synthetic and real data and compare our proposal against the state-of-the-art solvers under a wide variety of configurations. We also report the influence of our method in the performance of 2-view BA against the common initializations.

As an additional contribution, we release the code for this version of our work in

<https://github.com/mergarsal/FastCertRelPose.git>.

Notice that, although we show in Section (VII) that strong duality usually holds for the RPP and the chosen relaxations (from which our certifiers are derived), a formal proof of this behavior is not available yet.

Last, we want to point out that while our proposal estimates the essential matrix, the relative rotation and translation *up-to-scale* can be extracted from it by any classic computer vision algorithm [1].

## II. RELATED WORK

Here we summarized briefly the solvers proposed in the literature for the Relative Pose problem. For a more detailed list, we refer the reader to [13].

### A. Non-certifiable approaches

#### Closed-form solvers

The essential matrix has five degrees of freedom (three from 3D rotation, three from 3D translation and one less because the scale ambiguity) and therefore, only five correspondences (except for degenerate cases [1]) are required for its estimation. This is the so-called minimal problem and since it provides us with an efficient hypothesis generator, it can be embedded into a RANSAC framework to gain robustness against wrong correspondences, *i.e.* outliers [11], [22]. However, this minimal problem involves the resolution of a nontrivial (tenth degree) polynomial [19], [20], and the tools to solve it (*e.g.* polynomial ideal theory or Gröbner basis) are not always numerically stable. Hence, some previous works have proposed alternative approaches, see *e.g.* [40], [41].

In post of simplicity, the 8-point algorithm by Faugeras *et al.* [23], which was originally proposed for the fundamental

matrix, is usually adapted to the case of the essential matrix, *i.e.* calibrated cameras. Of significant importance is the extension of the 8-point algorithm that includes all the correspondences, usually known as the Direct Linear Transform (DLT) [1].

#### Iterative solvers

The above-mentioned solvers typically provide suboptimal solutions for the non-minimal N-point problem and therefore it is a common practice to refine these initial estimates by local, iterative methods [22]. Contrary to optimization problems on flat (Euclidean) spaces, these local optimization methods must respect the intrinsic constraints of the search space, *i.e.* the solution must be always an essential matrix. Different parameterizations for the set of essential matrices have been proposed, see *e.g.* [16], [17], [21], [26]. As it was shown in [17], these parameterizations may lead to different performances and convergence rates for non-linear optimization methods. The main difficulty relies on the peculiarities of the epipolar constraints and the symmetry between the two views, which are often not taking into account. The characterization proposed in [26] leverages the concept of quotient manifold [42] in order to model all these peculiarities. Nevertheless, simple characterizations (*e.g.*, the product space of 3D rotations and 2-sphere) may still work in most problem instances under some conditions, for example, a good initial guess.

### B. Certifiable approaches

#### Branch-and-Bound

Despite its attractiveness as fast solvers, the above-mentioned methods do not guarantee nor certify if the retrieved solution is optimal. In fact, finding said optimal solutions with guarantees for non-convex problems, such as the Relative Pose problem, is in general a hard task. Nonetheless, approaches with exponential time complexity in worst-case scenarios that rely on Branch-and-Bound global optimization have been proposed for that. In [43], the authors incorporated the presence of outliers as an inlier-set maximization problem. In [12], it was first proposed the estimation of the essential matrix under a  $L_\infty$  cost function. In [11], an eigenvalue formulation equivalent to the algebraic error was proposed and solved in practice by an efficient Levenberg-Marquardt scheme and a globally optimal Branch-and-Bound. However, Branch-and-Bound has a slow performance.

#### Convex Relaxation

A different approach that also certifies the optimality of the solution consists of the re-formulation of the original problem as a Quadratically Constrained Quadratic Program (QCQP). These problems are still NP-hard to solve in general; nonetheless we can relax these QCQPs into Semidefinite Relaxation Programs (SDPs) that can be actually solved in polynomial time by off-the-shelf tools, like SDPT3 [44] or SeDuMi [45].

One of these convex relaxations that have been shown to perform well in practice is known as the Shor's relaxation [46]. If the relaxation happens to be tight, one can recover the

solution to the original problem with an optimality certificate. This relaxation has been shown to remain tight for a wide variety of problems under some conditions and noise regimens, for example in generalized essential matrix estimation [47],  $n$ -view triangulation [48] or the Wahba problem with outliers [49], among others.

This was the approach followed in [27], in which the authors posed the RPP as an optimization problem that minimizes an objective function equivalent to the squared epipolar error directly over the rotation and translation spaces. In [15] the author proposed another Shor’s relaxation for the Relative Pose problem that minimizes the squared epipolar error but over the set of normalized essential matrices, leading to a small relaxation that was solved in roughly 6 *ms* under a C++ implementation. Although these approaches are faster than those based on BnB, they are still slow for the computer vision standard.

### Certifiable algorithms

Although tractable, solving these convex problems from scratch may not be the most efficient way to address them. As an alternative approach one may find the so-called Fast Certifiable Algorithms recently characterized and motivated in [28]. These algorithms typically leverage the existence of an optimality certifier which, given a solution obtained by any means, may be able to certify its optimality. A straightforward approach to get that certificate is through the resolution of the *dual problem* [46] from scratch, whose optimal cost value always provides a lower bound on the optimal objective for the original problem. In many real-world problem instances this bound is *tight*, meaning both cost values are the same up to some accuracy and one can certify optimality from it. Under some conditions, we can even extract the solution to our original problem from the solution of the dual, see *e.g.* [50] for extrinsic calibration of sensors or [31] for registration of points, lines and planes. However, this naive approach would still be as slow as directly solving the problem via its convex relaxation, since for the RPP as posed in [15], [27] both problems are instances of Positive Semidefinite problems (SDP) which can be solved up to arbitrary accuracy in polynomial time.

However, it is also possible to leverage the dual problem to derive a faster certification algorithm. This approach usually leads to a closed-form expression for dual candidates, that is, points that are feasible for the dual problem (within the domain of the dual function). This expression depends on the optimal solution for the original (primal) problem, and if the candidate is indeed feasible, it allows us to certify the optimality of the original solution. For QCQP, the feasibility of the dual candidates is reduced to a spectral analysis of the Hessian of the Lagrangian [46]. This has been the approach followed for other problems, for example, rotation averaging [29], point cloud registration with missing data [30] and outliers [38], pose graph optimization [51], [52] or SLAM [32]–[34].

Our previous work [13] proposed for the first time this kind of optimality certification for the Relative Pose problem. It was shown that the certifiable pipeline works in most problem

instances under a wide variety of regimes. Here, we improve this certifier, extend it to consider bad matches, *i.e.* outliers and evaluate the new proposal against the state-of-the-art solvers for the RPP in extensive experiments on both synthetic and real data.

### III. NOTATION

In order to make clearer the mathematical formulation in the paper, we first introduce the notation used hereafter. Bold, upper-case letters denote matrices, *e.g.*  $\mathbf{E}, \mathbf{C}$ ; bold, lower-case denotes (column) vectors, *e.g.*  $\mathbf{t}, \mathbf{x}$ ; and normal font letters denote scalars, *e.g.*  $a, b$ . We reserve  $\lambda$  for the Lagrange multipliers (Section (IV-B)) and  $\mu$  for eigenvalues. Additionally, we will denote with  $\mathbb{R}^{n \times m}$  the set of  $n \times m$  real-valued matrices,  $\mathbb{S}^n \subset \mathbb{R}^{n \times n}$  the set of symmetric matrices of dimension  $n \times n$  and  $\mathbb{S}_+^n$  the cone of positive semidefinite (PSD) matrices of dimension  $n \times n$ . A PSD matrix will be also denoted by  $\succeq$ , *i.e.*,  $\mathbf{A} \succeq 0 \Leftrightarrow \mathbf{A} \in \mathbb{S}_+^n$ . We denote by  $\otimes$  the Kronecker product and by  $\mathbf{I}_n$  the (square) identity matrix of dimension  $n$ . The operator  $\text{vec}(\mathbf{B})$  vectorizes the given matrix  $\mathbf{B}$  column-wise. We denote by  $[\mathbf{t}]_{\times}$  the matrix form for the cross-product with a 3D vector  $\mathbf{t} = [t_1, t_2, t_3]^T$ , *i.e.*,  $\mathbf{t} \times (\bullet) = [\mathbf{t}]_{\times}(\bullet)$  with

$$[\mathbf{t}]_{\times} = \begin{bmatrix} 0 & -t_3 & t_2 \\ t_3 & 0 & -t_1 \\ -t_2 & t_1 & 0 \end{bmatrix}. \quad (1)$$

Last, we employ the subindex  $R$  through this document to indicate a relaxation of the element w.r.t. the element without subindex. For example,  $\mathbb{E}_R$  stands for the set that is a relaxation of  $\mathbb{E}$  and therefore a superset of the latter, *i.e.*  $\mathbb{E}_R \supset \mathbb{E}$ .

We define the 2-sphere as  $\mathbb{S}^2 \doteq \{\mathbf{t} \in \mathbb{R}^3 | \mathbf{t}^T \mathbf{t} = 1\}$  and the set of (3D) rotation matrices as  $\text{SO}(3) \doteq \{\mathbf{R} \in \mathbb{R}^{3 \times 3} | \mathbf{R}^T \mathbf{R} = \mathbf{I}_3, \det(\mathbf{R}) = +1\}$ .

### IV. RPP FORMULATION AND CLOSED-FORM DUAL CANDIDATE

We consider the central calibrated Relative Pose problem in which one seeks the relative rotation  $\mathbf{R}$  and translation  $\mathbf{t}$  between two cameras, given a set of  $N$  pair-wise feature correspondences between the two images coming from these distinctive viewpoints, see Figure (1). In this work, the pair-wise correspondences are defined as pairs of (noisy) unit bearing vectors  $(\mathbf{f}_i, \mathbf{f}'_i)$  which, if they were a correct correspondence, should point from their respective camera centers towards the same 3D scene point. A traditional way to face this problem is by introducing the essential matrix  $\mathbf{E} = [\mathbf{t}]_{\times} \mathbf{R}$  [1], [53], a  $3 \times 3$  matrix that encapsulates the geometric information about the relative pose between two calibrated views. The essential matrix relates each pair of corresponding points through the *epipolar constraint*  $\mathbf{f}_i^T \mathbf{E} \mathbf{f}'_i = 0$ , provided that the observations are noiseless. With noisy data, however, the equality does not hold and  $\mathbf{f}_i^T \mathbf{E} \mathbf{f}'_i = \epsilon_i$  defines what is called the *normalized algebraic error*.

In this work we pose the RPP as an optimization problem over the set of essential matrices that minimizes the squared

algebraic error  $\epsilon^2$ , as it has been performed previously in the literature, *e.g.*, [15]–[17]. We write the cost function in terms of  $\mathbf{E}$  as a quadratic form via the positive semi-definite (PSD) matrix  $\mathbf{C} = \sum_{i=1}^N \mathbf{C}_i$ , with  $\mathbf{C}_i = (\mathbf{f}'_i \otimes \mathbf{f}_i)(\mathbf{f}'_i \otimes \mathbf{f}_i)^T \in \mathbb{S}_+^9$  and so, the problem reads:

$$f^* = \min_{\mathbf{E} \in \mathbb{E}} \sum_{i=1}^N (\mathbf{f}'_i^T \mathbf{E} \mathbf{f}_i)^2 = \min_{\mathbf{E} \in \mathbb{E}} \underbrace{\text{vec}(\mathbf{E})^T \mathbf{C} \text{vec}(\mathbf{E})}_{f(\mathbf{E})}. \quad (\text{O})$$

See [13, App. A] for a formal proof of the equivalence between the objective functions. In (O),  $\mathbb{E}$  stands for the set of (normalized) essential matrices, typically defined as

$$\mathbb{E} \doteq \{\mathbf{E} \in \mathbb{R}^{3 \times 3} \mid \mathbf{E} = [\mathbf{t}]_{\times} \mathbf{R}, \mathbf{R} \in \text{SO}(3), \mathbf{t} \in \mathcal{S}^2\}. \quad (2)$$

Note that in (2) the translation is identified with points in the 2-sphere due to the scale ambiguity for central cameras.

#### A. A Relaxation of the Set of Essential Matrices

For the purpose of this work, a minimal (quadratic) representation is preferred. We leverage the one proposed by Faugeras *et al.* in [23]:

$$\mathbb{E} \doteq \{\mathbf{E} \in \mathbb{R}^{3 \times 3} \mid \mathbf{E} \mathbf{E}^T = [\mathbf{t}]_{\times} [\mathbf{t}]_{\times}^T, \mathbf{t}^T \mathbf{t} = 1\}. \quad (3)$$

This parameterization, recently exploited by Zhao in [15], features a low number of variables (12) and constraints (7), and was proved to be useful in practice. Despite its advantages, this parameterization still does *not* allow for the development of a *fast optimality certifier* for the RPP in the fashion of that proposed for problems like Pose Graph Optimization, as in [32], [33].

To overcome this, in [13] we proposed a relaxed version  $\mathbb{E}_R$  of the essential matrix set  $\mathbb{E}$  by dropping one the constraints in (3), concretely  $\mathbf{e}_1^T \mathbf{e}_2 + t_1 t_2 = 0$ . This relaxed set is then defined as:

$$\mathbb{E} \subset \mathbb{E}_R \doteq \{\mathbf{E} \in \mathbb{R}^{3 \times 3} \mid h_i(\mathbf{E}, \mathbf{t}) = 0, \forall h_i \in \mathcal{C}_R; \mathbf{t} \in \mathbb{R}^3\}, \quad (4)$$

with  $\mathcal{C}_R$  the *relaxed constraint set* defined as

$$\mathcal{C}_R \equiv \begin{cases} h_1 \equiv \mathbf{t}^T \mathbf{t} - 1 = 0 \\ h_2 \equiv \mathbf{e}_1^T \mathbf{e}_1 - (t_2^2 + t_3^2) = 0 \\ h_3 \equiv \mathbf{e}_2^T \mathbf{e}_2 - (t_1^2 + t_3^2) = 0 \\ h_4 \equiv \mathbf{e}_3^T \mathbf{e}_3 - (t_1^2 + t_2^2) = 0 \\ h_5 \equiv \mathbf{e}_1^T \mathbf{e}_3 + t_1 t_3 = 0 \\ h_6 \equiv \mathbf{e}_2^T \mathbf{e}_3 + t_2 t_3 = 0 \end{cases}, \quad (5)$$

and the rows of  $\mathbf{E}$  have been denoted by  $\mathbf{e}_i \in \mathbb{R}^3, \forall i \in \{1, 2, 3\}$ . A formal proof of how  $\mathbb{E}_R$  in (4) defines a strict superset of  $\mathbb{E}$  is provided in [13, App. B].

We could have discarded any other constraint (except  $h_1$ ) and hence, obtained other similar yet different relaxed constraint sets. For the sake of simplicity, we will restrict ourselves to the set in (5) and we provide the general form of the certifier in Section (IV-C). The following development can be trivially adapted to any other relaxation of  $\mathbb{E}$ .

#### Relaxed Formulation of the Relative Pose Problem

With this relaxed set at hand, we define a *relaxed* version (R) of the original RPP in (O):

$$f_R^* = \min_{\mathbf{E} \in \mathbb{E}_R} \text{vec}(\mathbf{E})^T \mathbf{C} \text{vec}(\mathbf{E}). \quad (\text{R})$$

Since problem (R) is a relaxation of (O), the inequality  $f_R^* \leq f^*$  holds with equality only if the solution to (R) is also an essential matrix, and hence also feasible for (O). Interestingly enough though, we observed that equality holds ( $f_R^* = f^*$ ) in many problem instances in practice, meaning that the relaxed problem (R) is very often a tight relaxation of the original problem (O). We have no theoretical proof as to why the behavior above holds so often, and our support to this claim is fundamentally empirical (given by extensive experiments in Section (VII)).

#### B. Closed-form Expression for Dual Candidates

To derive our certifier, we first re-formulate the relaxed problem (R) as a standard instance of QCQP by writing explicitly the constraints in  $\mathcal{C}_R$ . For that, we define the 12-D vector  $\mathbf{x} = [\mathbf{e}^T, \mathbf{t}^T]^T$ , with  $\mathbf{e} = \text{vec}(\mathbf{E})$  and hence:

$$f_R^* = \min_{\mathbf{x} \in \mathbb{R}^{12}} \mathbf{x}^T \mathbf{Q} \mathbf{x} \quad \text{subject to } \mathbf{x}^T \mathbf{A}_i \mathbf{x} = c_i, i = 1, \dots, 6 \quad (\text{P-R})$$

where  $\{\mathbf{A}_i\}_{i=1}^6$  are the  $12 \times 12$ -symmetric corresponding matrix forms of the quadratic constraints, so that  $h_i(\mathbf{E}, \mathbf{t}) \equiv \mathbf{x}^T \mathbf{A}_i \mathbf{x} - c_i = 0, c_i \in \mathbb{R}$  with  $c_1 = 1$  and  $c_i = 0$  for  $i = 2, \dots, 6$ , and  $\mathbf{Q}$  is the  $12 \times 12$ -symmetric data matrix of compatible dimension with  $\mathbf{x}$  padded with zeros.

Problem (P-R) is exactly equivalent to the relaxed Problem (R). Nonetheless, Problem (P-R) is still a Quadratically Constrained Quadratic Program (QCQP), in general NP-hard to solve. However, it allows us to derive an optimality certifier by exploiting the so-called *Lagrangian dual problem* [46], that takes the form:

$$d_R^* = \max_{\boldsymbol{\lambda}} \lambda_1 \quad \text{subject to } M(\boldsymbol{\lambda}) \succeq 0 \quad (\text{D-R})$$

where  $M(\boldsymbol{\lambda}) \doteq \mathbf{Q} - \sum_{i=1}^6 \lambda_i \mathbf{A}_i$  is the so-called *Hessian of the Lagrangian* and  $\boldsymbol{\lambda} = \{\lambda_i\}_{i=1}^6$  are the *Lagrange multipliers*. The derivation of the problem is given in [13, App. C].

The dual problem (D-R) presents a relaxation of the primal program (P-R) and hence, its objective cost  $d_R(\hat{\boldsymbol{\lambda}})$  provides us with a lower bound for the objective of the latter  $f_R(\hat{\mathbf{x}})$ , principle known as *weak duality* [46]. Consider a feasible dual point  $\hat{\boldsymbol{\lambda}}$ , *i.e.* a point that fulfills the constraints required by the dual problem, for (D-R) and a feasible primal point  $\hat{\mathbf{x}}$  for the relaxed primal in (P-R). The objective costs attain by this pair of primal/dual points ( $f_R(\hat{\mathbf{x}}), d_R(\hat{\boldsymbol{\lambda}})$ , respectively) are related by the following chain of inequalities:

$$d_R(\hat{\boldsymbol{\lambda}}) \stackrel{a}{\leq} d_R^* \stackrel{b}{\leq} f_R^* \stackrel{c}{\leq} f^* \stackrel{d}{\leq} f(\hat{\mathbf{E}}), \quad (6)$$

where (a) and (d) hold by definition of optimality, (c) stands since (P-R) is a relaxation of (O) and (b) holds because, at

the same time, the dual problem is a relaxation of the primal (P-R) (*weak duality*).

From (6) we can see that the dual problem allows to certify if a given primal feasible point  $\hat{x}$  is indeed optimal. If for a pair of primal/dual feasible points we have that  $f_R(\hat{x}) = d_R(\hat{\lambda})$  (up to some accuracy), then the chain of inequalities becomes tight and  $f^* = f_R(\hat{x})$ , which shows that  $\hat{x}$  is the optimal solution. In these cases, we say that there is *strong duality* and that the *duality gap*  $f_R^* - d_R^*$  is zero.

Although the dual problem (D-R) is a SDP and can be solved by off-the-shelf solvers (e.g., SeDuMi [45] or SDPT3 [44]) in polynomial time, a faster optimality verification can be derived. This certification relies on a closed-form expression for dual candidates  $\hat{\lambda}$ , thus avoiding the resolution of the SDP from scratch. This closed-form expression is derived from the requirement that every primal solution  $\hat{x}$  must fulfill the KKT conditions [46, Sec. 5.5].

**Theorem IV.1** (Verification of Optimality [13, Th. 5.2]). *Given a putative primal solution  $\hat{x}$  for Problem (P-R), if there exists a solution  $\hat{\lambda}$  to the linear system*

$$J(\hat{x})\hat{\lambda} = Q\hat{x}, \quad (7)$$

and  $M(\hat{\lambda}) \succeq 0$ , then we have strong duality and the putative solution  $\hat{x}$  is indeed optimal. Here  $J(\hat{x}) \in \mathbb{R}^{12 \times 6}$  is the full-rank Jacobian of the constraints evaluated at the potentially optimal point  $\hat{x}$  for the relaxed problem (P-R) whose explicit form can be found in [13] and in the Online Resource Section (A).

The restriction of Theorem (IV.1) to essential matrices is summarized as follows:

**Corollary IV.1.1.** [13, Cor. 5.2.1] *Given a potentially optimal solution  $\hat{E}$  for problem (O) and its equivalent form  $\hat{x} = [\text{vec}(\hat{E})^T, \hat{t}^T]^T$  where  $\hat{t}$  is the associated translation vector, if there exists a unique solution  $\hat{\lambda}$  to the linear system in (7) and it is dual feasible (i.e.  $M(\hat{\lambda}) \succeq 0$ ), then we can state that: (1) strong duality holds between problems (P-R) and (D-R); (2) the relaxation carried out in (P-R) is tight; and (3) the potentially optimal solution  $\hat{E}$  is optimal for both (P-R) and (O).*

We want to point out that Theorem (IV.1) and Corollary (IV.1.1) can only either certify the given primal solution is indeed optimal, or it is inconclusive about its optimality. The reason for the latter is associated either with a suboptimal solution and/or a loose relaxation (either the one carried out for the primal in (P-R) and/or the one for the dual in (D-R)).

**Remark 1.** *In this work we propose a set of six relaxations of the original problem (O) obtained by dropping only one constraint from the original set in (3). These relaxations allow to compute a unique dual candidate  $\hat{\lambda}$  in closed-form from (7) since the Jacobian is full rank. We can, nevertheless, discard more constraints and still derive closed-form expressions for dual candidates and the associated fast certification algorithms akin to Theorem (IV.1). These problems, though,*

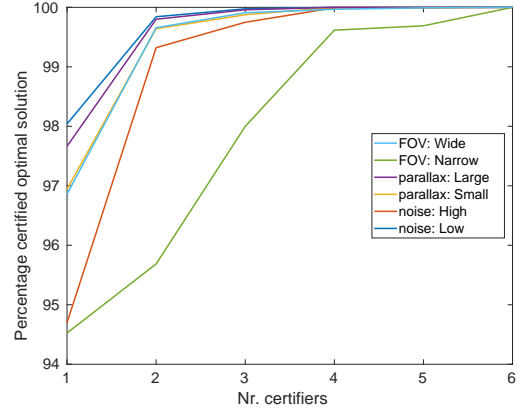


Fig. 3: Cumulative percentage of cases with certified solutions as a function of the number of computed certifiers for regimes with different noise, parallax and field of view. “Parallax: Small” and “FOV: Wide” overlap in the figure.

are looser relaxations of the original (O), and their dual problems may not provide with a tight lower bound, that is, the certifier associated to that relaxation will not be able to certify the optimal solution to the original problem. While the computation cost for these smaller certifiers could be potentially lower (the linear system in (7) has fewer unknowns  $\hat{\lambda}$ ), we do not know a priori whether any of these relaxations perform well in terms of certification of essential matrices. Therefore, the tightest relaxations for the parameterization of the essential matrix set in (3) that still assure closed-form expressions with unique solution for dual candidates are obtained by dropping only one constraint of the set.

### C. Family of Certifiers from different Closed-form Dual Candidates

The employed relaxation of the feasible set of essential matrices in (5) was necessary in order to assure the uniqueness of the Lagrange multipliers. We can, nevertheless, obtain similar yet different relaxations by dropping one of the other five different constraints in  $EE^T$ . These relaxations would yield distinct optimality certifiers for the same problem whose candidates to Lagrange multipliers are also computed in closed-form. If (at least) one of them fulfills the conditions for optimality (see Theorem (IV.1)), then the solution is optimal and the associated underlying relaxation is tight. On the other hand, if none of them fulfill these conditions, this does not imply that the solution is suboptimal: all the relaxations could be not tight at the same time as well. In its general form, we can write the closed-form expression for the multipliers as:

$$Q\hat{x} = \sum_{i=2}^7 \theta_i \hat{\lambda}_i A_i \hat{x} + \hat{\lambda}_1 A_1 \hat{x} = J(\hat{x}, \theta)\hat{\lambda}, \quad (8)$$

where  $\theta_i \in \{0, 1\}$ ,  $i = 2, \dots, 7$ , with  $\sum_i \theta_i = 5$  and  $\theta \doteq [\theta_2, \dots, \theta_7]$ . The variable  $\theta_i$  “activates” the  $i$ -th constraint

(with matrix form  $\mathbf{x}^T \mathbf{A}_i \mathbf{x} = c_i$ ,  $i = 2, \dots, 7$ ) when it is equal to one. In other terms, for any combination of  $\theta$ , one of the constraints in (3) (except  $h_i$ ) is always deactivated. The column of the full Jacobian associated with that multiplier is zero for any point  $\hat{\mathbf{x}}$  and it can be dropped. Hence, the matrix  $\mathbf{J}(\hat{\mathbf{x}}, \theta)$  has always linearly independent columns (following a similar proof to that provided in [13, App. D]).

In the worst case, we compute six different certifiers: solve Equation (8) with the six different combinations for  $\theta$ ; and six eigenvalues of a  $3 \times 3$  matrix (closed-form) and six eigenvalues of a  $9 \times 9$  matrix. In practice, however, this is not necessary. Figure (3) depicts the cumulative percentage of cases with certified optimal solutions (Y-axis) as a function of the number of computed certifiers (X-axis) for different level of noise, parallax and Field of View (Section (VII) explains the details about the experiments). Note that at least 99% of optimal cases are detected with only 2 certifiers for most of the problems (except narrow field of views, FOV), while the 100% is detected with 4 certifiers. For narrow FOV 70 – 90 degrees, however, one may need to compute all of them.

This redundant estimation of potential dual candidates increases the computation time required by the verification stage. We observe that estimating the Lagrange multipliers and checking the spectral conditions takes approximately the same amount of time that the initialization by the 8-PT algorithm (singular vector estimation and projection). We can, of course, compute only one certifier. As it is shown in Figure (3), we will still detect more than 95% of the optimal cases in general. The choice is left to the user and the application.

#### D. Exploiting structure: separating and ordering

Once the candidate has been computed, Theorem (IV.1) requires to analyze the eigenvalues of the Hessian of the Lagrangian  $M(\hat{\lambda})$ . This matrix is block-diagonal with two (squared) blocks  $M^e(\hat{\lambda}), M^t(\hat{\lambda})$  of size 9 and 3, respectively. Both blocks must be positive semi-definite (PSD) for the full Hessian to be PSD, since the spectrum of a block-diagonal matrix is the union of the spectra of its blocks. We can then translate the original condition  $M(\hat{\lambda}) \succeq 0$  to the two smaller conditions  $M^e(\hat{\lambda}) \succeq 0$  and  $M^t(\hat{\lambda}) \succeq 0$ , which must hold at the same time. Further, and although our justification here is purely empirical, we observe that those cases for which the Hessian was not PSD were associated with  $M^t(\hat{\lambda})$  being not PSD. Therefore and in practice, we check first the PSD condition for this  $3 \times 3$  matrix (whose eigenvalues have a closed-form expression). If it is fulfilled, we then verify the condition for  $M^e(\hat{\lambda})$ . If both blocks are PSD, then the Hessian is PSD.

With these improvements at hand, we can now provide the optimality certification algorithm in Algorithm (1). To universalize the Algorithm, let us denote by  $\hat{\mathbf{x}} = [\text{vec}(\hat{\mathbf{E}})^T, \hat{\mathbf{t}}^T]^T$  the feasible solution for (P-R) or for (O). Further, for any  $\hat{\mathbf{E}} \in \mathbb{E}$ , the attained objective value in (O) ( $f(\hat{\mathbf{E}})$ ) agrees with the objective value in (P-R) ( $f_R(\hat{\mathbf{x}})$ ) since  $\mathbb{E} \subset \mathbb{R}_R$ ; hence we employ  $f_R(\hat{\mathbf{x}})$  to denote the corresponding objective value

---

#### Algorithm 1: Optimality Certification

---

```

1  Input: Compact data matrix  $\mathbf{C}$ ; primal solution  $\hat{\mathbf{x}}$ 
2  Output: Optimality certificate ISOPT
    $\in \{\text{True}, \text{unknown}\}$ 
3  Compute  $f_R(\hat{\mathbf{x}})$  from (P-R);
4   $\text{idxRelaxation} \leftarrow 1$ ;
5  repeat
   // For the i-th relaxation
6  Compute  $\hat{\lambda}$  by solving the linear system in (7) and
   set  $d_R(\hat{\lambda}) = \hat{\lambda}_1$ ;
7  Compute min. eigenvalue  $\mu_t$  of  $M^t(\hat{\lambda})$ ;
8  if  $\mu_t \leq \tau_\mu$  or  $|f_R(\hat{\mathbf{x}}) - d_R(\hat{\lambda})| > \tau_{\text{gap}}$  then
   // Dual candidate is not
   // feasible
9  ISOPT = unknown;
10  $\text{idxRelaxation} \leftarrow \text{idxRelaxation} + 1$ ;
11 else
12 Compute min. eigenvalue  $\mu_E$  of  $M^e(\hat{\lambda})$ ;
13 if  $\mu_E \leq \tau_\mu$  or  $|f_R(\hat{\mathbf{x}}) - d_R(\hat{\lambda})| > \tau_{\text{gap}}$  then
   // Dual candidate is not
   // feasible
14 ISOPT = unknown;
15  $\text{idxRelaxation} \leftarrow \text{idxRelaxation} + 1$ ;
16 else
17 // Dual candidate is feasible
   ISOPT = True;
18 until ISOPT is TRUE or  $\text{idxRelaxation}$  is 6;
```

---

in both cases without confusion. Recall that our certification has two possible outcomes, either POSITIVE (the solution is optimal) or UNKNOWN (the certification is inconclusive). From a practical point of view, we write the conditions  $M^e(\hat{\lambda}), M^t(\hat{\lambda}) \succeq 0$  as their smallest eigenvalues  $\mu_t, \mu_E$  being greater than a negative threshold  $\tau_\mu$ . Further, while our closed-form certifier assumes that strong duality holds, due to rounding errors the dual gap  $f_R(\hat{\mathbf{x}}) - d_R(\hat{\lambda})$  may not be exactly zero. We assure strong duality by applying a (positive) threshold  $\tau_{\text{gap}}$  to the absolute value of the dual gap  $|f_R(\hat{\mathbf{x}}) - d_R(\hat{\lambda})|$ , which allow us to accommodate numerical errors. In practice, we fix the tolerances to  $\tau_\mu = -0.02$  and  $\tau_{\text{gap}} = 10^{-14}$ . If any of the minimum eigenvalues are negative and/or the dual gap is greater than zero (considering the tolerance in both cases), the certification procedure is inconclusive.

#### V. PROPOSED FAST CERTIFIABLE PIPELINE

Rather than solving the original problem (O) via its convex SDP relaxation, in this work we propose to solve the RPP through an iterative method that respects the intrinsic nature of the essential matrix set, but comes with no optimality guarantees, and to certify *a-posteriori* the optimality of the solution leveraging our fast optimality certifier in Algorithm (1). Current iterative methods work well and usually converge to

the global optima in addition to be faster than the methods employed in convex programming, *e.g.*, Interior Point Methods (IPM). Following, we enumerate and briefly explain the three major stages in which the proposed pipeline is separated:

- 1) **Initialization:** We start by generating an initial guess with any standard algorithm, *e.g.* the 8-PT algorithm [1].
- 2) **Refinement (optimization on manifold):** We seek the solution to the original primal problem (O) by refining the initial guess with a local iterative method that operates within the essential matrix manifold  $\mathcal{M}_E$  (always fulfilling constraints).

$$\hat{E} = \arg \min_{E \in \mathcal{M}_E} \text{vec}(E)^T C \text{vec}(E). \quad (9)$$

Recall that the matrix  $Q \in \mathbb{S}_+^{12}$  is the data matrix  $C \in \mathbb{S}_+^9$  padded with zeros.

- 3) **Verification of optimality:** The candidate solution  $\hat{E}$  returned by the iterative method can be certified as the global optimum with the proposed Algorithm (1) if the underlying dual problem (D-R) is tight.

Note that the above-mentioned pipeline estimates the essential matrix, which encodes the relative pose. Both the rotation and translation *up-to-scale* can be extracted from it by any classic computer vision algorithm [1].

#### A. Refinement of the initial estimation: optimization on manifold

Riemannian optimization toolboxes decouple the optimization problem into manifold (domain), problem description and solvers, thus making it quite straightforward to implement an iterative solver for (9) as proposed above.

**Domain:** Current tools for optimization on manifolds, such as MANOPT [54], provide a wide variety on pre-defined manifolds and operators which alleviate the programming effort required for its use. Although the implementation is pretty simple when the employed manifold is supplied by the tool (as it happens in [13]), this is not always the case. In those situations, the user needs to either implement it or employ a different but equivalent parameterization of the manifold whose components are provided by the library.

In the RPP the essential matrix manifold can be simplified in most cases to the direct product space  $\text{SO}(3) \times \mathcal{S}^2$  by leveraging the standard definition given in (2). This product is composed of two well-known spaces,  $\text{SO}(3)$ ,  $\mathcal{S}^2$ , which are usually provided by the optimization toolboxes. In any case, they can be also easily implemented, so is their direct product (see *e.g.* [16]).

Despite its simplicity, however, the above-mentioned product is indeed a four-fold covering of the essential matrix manifold  $\mathcal{M}_E$  (ambiguity which is well-known [1], [27]). Nevertheless, this does not suppose a major issue when we are only required to estimate one single essential matrix at a time (manifold optimization); we refer the reader to [26] for a full characterization of  $\mathcal{M}_E$  and to [55] for a detailed explanation of those cases in which this simplification cannot be employed directly (manifold statistics).

Although simple, this re-parameterization of the search space requires to adapt the objective function to the new set of variables, which may not be straightforward. Further, we also need to provide the gradient and the Hessian (if the chosen solver employs second-order information) w.r.t. this new parameterization. Thanks to the decoupling of the problem into domain and model description, the well-known nature of the rotation and sphere groups and the simplification of the product of manifolds, there exist simple relations between the ambient gradient and Hessian-vector product and their Riemannian counterparts. First, let the objective function  $f(\mathbf{R}, \mathbf{t})$  be defined in terms of the rotation and translation  $(\mathbf{R}, \mathbf{t})$  (to be defined later). The Riemannian gradient  $\text{grad}f(\mathbf{R}, \mathbf{t})$  and Hessian-vector product  $\text{Hess}_{\mathbf{R}, \mathbf{t}}f(\mathbf{R}, \mathbf{t})$  defined on the space  $\text{SO}(3) \times \mathcal{S}^2$  can be treated element-wise, that is:  $\text{grad}f(\mathbf{R}, \mathbf{t}) = (\text{grad}_{\mathbf{R}}f(\mathbf{R}, \mathbf{t}), \text{grad}_{\mathbf{t}}f(\mathbf{R}, \mathbf{t}))$ , where the two terms are the Riemannian gradients w.r.t.  $\mathbf{R}$  and  $\mathbf{t}$ , respectively. Similarly, the Riemannian Hessian-vector product is defined as  $\text{Hess}_{\mathbf{R}, \mathbf{t}}f(\mathbf{R}, \mathbf{t}) = (\text{Hess}_{\mathbf{R}}f(\mathbf{R}, \mathbf{t}), \text{Hess}_{\mathbf{t}}f(\mathbf{R}, \mathbf{t}))$ , with the same notation than with the gradient. Hence, we only need to treat each component individually.

**Gradient:** By considering the objective function  $f(\mathbf{R}, \mathbf{t})$  as a function restricted to the embedded submanifold  $\text{SO}(3) \times \mathcal{S}^2 \subset \mathbb{R}^{3 \times 3} \times \mathbb{R}^3$ , we can define each term in the Riemannian gradient

$\text{grad}f(\mathbf{R}, \mathbf{t}) = (\text{grad}_{\mathbf{R}}f(\mathbf{R}, \mathbf{t}), \text{grad}_{\mathbf{t}}f(\mathbf{R}, \mathbf{t}))$  as the *orthogonal projection* to the tangent space of the corresponding Euclidean gradient  $(\nabla_{\mathbf{R}}f(\mathbf{R}, \mathbf{t}), \nabla_{\mathbf{t}}f(\mathbf{R}, \mathbf{t}))$  [42, Eq. 3.37], *i.e.*,

$$\begin{aligned} \text{grad}_{\mathbf{R}}f(\mathbf{R}, \mathbf{t}) &= \text{Proj}_{\mathbf{R}}(\nabla_{\mathbf{R}}f(\mathbf{R}, \mathbf{t})) \\ \text{grad}_{\mathbf{t}}f(\mathbf{R}, \mathbf{t}) &= \text{Proj}_{\mathbf{t}}(\nabla_{\mathbf{t}}f(\mathbf{R}, \mathbf{t})) \end{aligned} \quad (10)$$

The orthogonal projection operator  $\text{Proj}_{\mathbf{R}}(\bullet)$  onto the tangent space of  $\text{SO}(3)$  ( $\text{T}_{\mathbf{R}}$ ) at the point  $\mathbf{R}$  is defined as [42]

$$\text{Proj}_{\mathbf{R}} : \text{T}_{\mathbf{R}}(\mathbb{R}^{3 \times 3}) \longrightarrow \text{T}_{\mathbf{R}}(\text{SO}(3)) \quad (11)$$

$$\text{Proj}_{\mathbf{R}}(\mathbf{X}) = \mathbf{R} \text{skew}(\mathbf{R}^T \mathbf{X}), \quad (12)$$

where  $\text{skew}(\mathbf{A})$  extracts the skew-symmetric part of the matrix  $\mathbf{A}$ , *i.e.*  $\text{skew}(\mathbf{A}) = \frac{1}{2}(\mathbf{A} - \mathbf{A}^T)$ . Similarly for the translation term, the orthogonal projection operator  $\text{Proj}_{\mathbf{t}}(\bullet)$  onto the tangent space of  $\mathcal{S}^2$  ( $\text{T}_{\mathbf{t}}$ ) at the point  $\mathbf{t}$  is

$$\text{Proj}_{\mathbf{t}} : \text{T}_{\mathbf{t}}(\mathbb{R}^3) \longrightarrow \text{T}_{\mathbf{t}}(\mathcal{S}^2) \quad (13)$$

$$\text{Proj}_{\mathbf{t}}(\mathbf{x}) = \mathbf{x} - (\mathbf{t}^T \mathbf{x}) \mathbf{t}. \quad (14)$$

**Hessian-vector product:** Similarly, the two components of the Riemannian Hessian-vector product

$\text{Hess}_{\mathbf{R}}f(\mathbf{R}, \mathbf{t})$  and  $\text{Hess}_{\mathbf{t}}f(\mathbf{R}, \mathbf{t})$  are computed as the orthogonal projections of the ambient directional derivative of the gradient vector fields  $\text{grad}_{\mathbf{R}}f(\mathbf{R}, \mathbf{t})$ ,  $\text{grad}_{\mathbf{t}}f(\mathbf{R}, \mathbf{t})$  in the direction of  $\dot{\mathbf{R}}, \dot{\mathbf{t}}$ , respectively [42, Eq. 5.15]:

$$\text{Hess}_{\mathbf{R}}(\mathbf{R}, \mathbf{t})[\dot{\mathbf{R}}, \dot{\mathbf{t}}] = \text{Proj}_{\mathbf{R}} \left( \nabla_{\mathbf{R}}^2 f(\mathbf{R}, \mathbf{t})[\dot{\mathbf{R}}, \dot{\mathbf{t}}] - \dot{\mathbf{R}}^T \text{sym}(\mathbf{R} \nabla_{\mathbf{R}} f(\mathbf{R}, \mathbf{t})) \right) \quad (15)$$

$$\text{Hess}_{\mathbf{t}}(\mathbf{R}, \mathbf{t})[\dot{\mathbf{R}}, \dot{\mathbf{t}}] = \text{Proj}_{\mathbf{t}} \left( \nabla_{\mathbf{t}}^2 f(\mathbf{R}, \mathbf{t})[\dot{\mathbf{R}}, \dot{\mathbf{t}}] - (\dot{\mathbf{t}}^T \nabla_{\mathbf{t}} f(\mathbf{R}, \mathbf{t})) \dot{\mathbf{t}} \right), \quad (16)$$

where  $\text{sym}(\mathbf{A})$  extracts the symmetric part of the matrix  $\mathbf{A}$  i.e.,  $\text{sym}(\mathbf{A}) = \frac{1}{2}(\mathbf{A} + \mathbf{A}^T)$ .

**Quadratic Model of the Problem:** With this in mind, we show next how to write the original objective function in (P-R) in terms of the elements  $(\mathbf{R}, \mathbf{t}) \in \text{SO}(3) \times \mathcal{S}^2$  and provide the Euclidean gradient and Hessian-vector product. The following Theorem allows us to express the original quadratic cost function in terms of the points  $(\mathbf{R}, \mathbf{t}) \in \text{SO}(3) \times \mathcal{S}^2$  in two different and equivalent ways.

**Theorem V.1** (Equivalent expressions for the cost function in (P-R)). *The original cost function has the two following equivalent forms as functions of  $\mathbf{R}, \mathbf{t}$*

$$\frac{1}{2} \mathbf{e}^T \mathbf{C} \mathbf{e} = \frac{1}{2} \mathbf{t}^T \mathbf{M}_{\mathbf{t}} \mathbf{t} = \frac{1}{2} \mathbf{r}^T \mathbf{M}_{\mathbf{R}} \mathbf{r} \quad (17)$$

where  $\mathbf{e} = \text{vec}(\mathbf{E}) \in \mathbb{R}^9$ ,  $\mathbf{r} = \text{vec}(\mathbf{R}) \in \mathbb{R}^9$ ,

$$\mathbf{M}_{\mathbf{R}}(\mathbf{t}) \doteq (\mathbf{I}_3 \otimes [\mathbf{t}]_{\times})^T \mathbf{C} (\mathbf{I}_3 \otimes [\mathbf{t}]_{\times}) \in \mathbb{S}^9 \quad (18)$$

$$\mathbf{M}_{\mathbf{t}}(\mathbf{R}) \doteq \mathbf{B}^T (\mathbf{R}^T \otimes \mathbf{I}_3)^T \mathbf{C} (\mathbf{R}^T \otimes \mathbf{I}_3) \mathbf{B} \in \mathbb{S}^3, \quad (19)$$

being  $\mathbf{B}$  a sparse matrix such that  $\text{vec}([\mathbf{t}]_{\times}) = \mathbf{B} \mathbf{t}$  holds for any  $\mathbf{t} \in \mathbb{R}^3$ . Their full development from the original quadratic cost function, as well as their relation with previous works [27], [11] are given in the Online Resource Section (B).

From Theorem (V.1), we can derive the (Euclidean) gradient and Hessian required to define the quadratic model of the problem in a straightforward manner.

**Theorem V.2** (Euclidean Gradient and Hessian in  $\mathbb{R}^{3 \times 3} \times \mathbb{R}^3 \supset \text{SO}(3) \times \mathcal{S}^2$ ). *From Theorem (V.1), the (Euclidean) gradient  $\nabla f(\mathbf{R}, \mathbf{t}) \in \mathbb{R}^{12}$  and Hessian-vector product  $\nabla^2 f(\mathbf{R}, \mathbf{t})[\dot{\mathbf{R}}, \dot{\mathbf{t}}] \in \mathbb{R}^{12}$  are defined as:*

$$\nabla f(\mathbf{R}, \mathbf{t}) = \begin{pmatrix} \nabla_{\mathbf{R}} f(\mathbf{R}, \mathbf{t}) \\ \nabla_{\mathbf{t}} f(\mathbf{R}, \mathbf{t}) \end{pmatrix} = \begin{pmatrix} \mathbf{M}_{\mathbf{R}} & \mathbf{0}_{9 \times 3} \\ \mathbf{0}_{3 \times 9} & \mathbf{M}_{\mathbf{t}} \end{pmatrix} \begin{pmatrix} \mathbf{r} \\ \mathbf{t} \end{pmatrix} \quad (20)$$

$$\begin{aligned} \nabla^2 f(\mathbf{R}, \mathbf{t})[\dot{\mathbf{R}}, \dot{\mathbf{t}}] &= \begin{pmatrix} \nabla_{\mathbf{R}}^2 f(\mathbf{R}, \mathbf{t})[\dot{\mathbf{R}}, \dot{\mathbf{t}}] \\ \nabla_{\mathbf{t}}^2 f(\mathbf{R}, \mathbf{t})[\dot{\mathbf{R}}, \dot{\mathbf{t}}] \end{pmatrix} \\ &= \begin{pmatrix} \mathbf{M}_{\mathbf{R}} & \mathbf{M}_{\mathbf{t}, \mathbf{R}} \\ \mathbf{M}_{\mathbf{t}, \mathbf{R}}^T & \mathbf{M}_{\mathbf{t}} \end{pmatrix} \begin{pmatrix} \dot{\mathbf{r}} \\ \dot{\mathbf{t}} \end{pmatrix} \end{aligned} \quad (21)$$

where  $\mathbf{M}_{\mathbf{R}}, \mathbf{M}_{\mathbf{t}}$  are the symmetric matrices defined above.  $\mathbb{R}^{9 \times 3} \ni \mathbf{M}_{\mathbf{t}, \mathbf{R}} \doteq \mathbf{M}_{\mathbf{t}, \mathbf{R}}(\mathbf{R}, \mathbf{t})$  is provided in the Online Resource Section (C).

**Solver:** We choose here an iterative *truncated-Newton Riemannian trust-region* (RTR) solver [42]. RTR has shown before [51], [52] a very good trade-off between a large basin of convergence and superlinear convergence speed.

In order to speed up the converge of the algorithm and inspired by [51] and [52], we propose a suitable Hessian preconditioner for the relative pose problem which is proved through extensive experiments in Section (VII) to reduce the number of iterations required by the solver to converge. The use of a preconditioner is based on the dependence of the convergence rate of the conjugate method when solving the linear system  $\mathbf{A} \mathbf{x} = \mathbf{b}$  with the condition number of the matrix  $\mathbf{A}$ . The *Riemannian* preconditioner  $\mathbf{P}$  must be a linear, symmetric and positive definite operator from the tangent space of the manifold to itself. We propose to use the preconditioning operator similar to Jacobi and of the form

$$\mathbf{P}(\mathbf{U}) \doteq \text{Proj}_{\text{SO}(3) \times \mathcal{S}^2} \left( \frac{1}{\alpha} \mathbf{U} \right), \quad (22)$$

with  $\alpha$  is a positive scalar related to the eigenvalues of the data matrix  $\mathbf{C}$ . Since the data matrix cannot be zero and it is PSD, this preconditioner is, by definition, linear, symmetric and positive definite. It is also defined from and onto the tangent space since  $\mathbf{U}$  belongs to this tangent space and the result is projected onto the tangent space. We propose the value for  $\alpha = \lambda_1 + \lambda_2 + \lambda_3$ , which are the three largest eigenvalues of the data matrix  $\mathbf{C}$ . Although this preconditioner is heuristic, it is showcased later on Section (VII) that it does reduce the computation time for the iteration method, specially when the number of correspondences is large, as it is usually the case in practical applications.

## VI. ROBUST RESOLUTION OF THE RELATIVE POSE PROBLEM

Section (V) outlines a complete certifiable pipeline for the essential matrix estimation whose core lies on the local refinement stage. This refinement is, however, very sensitive to bad correspondences, i.e. outliers; in the presence of only one outlier, the solution will be biased. Instead of embedding and adjusting our pipeline into a RANSAC paradigm, we leverage the tools known as Graduated Non-convexity (GNC) [36] and the Black-Rangarajan duality [37] to detect and discard outliers. This scheme has been previously employed, see e.g. [15], [39], showing that it is able to estimate better solutions than RANSAC-based paradigms, specially for problem instances where the percentage of outliers is large. In this Section we summarize this scheme and specialized it for the Tukey's biweight loss function [37]. The approach is extensible to other functions, some of them can be also found in previous works (e.g., Welsch function in [15] and Truncated Least Square and Geman-McClure in [39]).

We first introduce a robust loss function  $\rho(\bullet)$  into the cost function  $f(\mathbf{E})$  of the original problem (O). The robust variant of (O) is written as

$$\min_{\mathbf{E} \in \mathbb{E}} \sum_{i=1}^N \rho(\epsilon_i), \quad (23)$$

where recall that  $\epsilon_i$  was the epipolar error for the  $i$ -th correspondence.

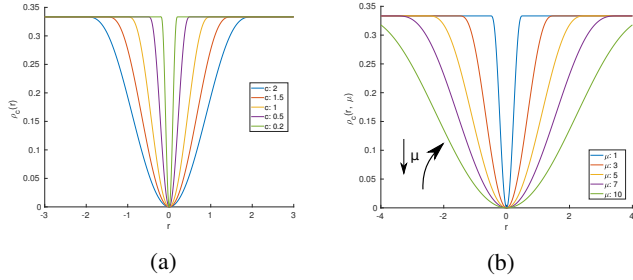


Fig. 4: Tukey's biweight function for different  $\bar{c}$  (24) (a); and its associated GNC functions for varying  $\mu$  (26) (b). In (b), we depict  $\bar{c} = 0.5$ .

It is known that the chosen loss function  $\rho$  has a great impact on the performance of the algorithm. Thus, although convex functions exist, such as Huber or  $\ell_1$ , these have a low breakdown point and are still sensible to gross outliers; non-convex loss functions are usually preferred. Following the approach in [39], we define the Tukey's biweight loss function  $\rho_{\bar{c}}(\bullet)$  in terms of a threshold  $\bar{c} \in \mathbb{R}$  as

$$\rho_{\bar{c}}(r) = \begin{cases} \frac{r^2}{\bar{c}^2} - \left(\frac{r^2}{\bar{c}^2}\right)^2 + \frac{1}{3}\left(\frac{r^2}{\bar{c}^2}\right)^3, & |r| \leq \bar{c} \\ \frac{1}{3}, & \text{otherwise} \end{cases}, \quad (24)$$

where  $\bar{c}$  determines the shape of the function, as it is shown in Figure (4a). The variable  $\bar{c}$  thus controls what points we are considering as inliers; for  $\bar{c}$  large, all the points are considered as such (including outliers), while in the opposite extreme, only these points with very low residuals are considered as inliers.

Since the loss function is non-convex, Problem (23) is prone to get trapped in local minima. The first step towards the efficient resolution of Problem (23) leverages the Black-Rangarajan duality between robust and line processes [37]. By introducing a set of slack variables or *weights*,  $w_i \in [0, 1]$ , one for each correspondence and an *outlier process* term  $\Psi_{\bar{c}}(w_i)$ , we can re-formulate any robust estimation problem as

$$\min_{\substack{\mathbf{E} \in \mathbb{E}, \\ w_i \in [0, 1], i=1, \dots, N}} \sum_{i=1}^N w_i \epsilon_i^2 + \Psi_{\bar{c}}(w_i). \quad (25)$$

The term  $\Psi_{\bar{c}}(w_i)$  that penalizes the weight  $w_i$  usually admits an analytical expression for most common loss functions (see [37]).

However, (25) is still non-convex. To avoid this behavior, we leverage the tool known as Graduated Non-convexity (GNC) that allows to optimize a generic non-convex function by solving a sequence of surrogate problems of increasing non-convexity. This is achieved by introducing a surrogate function  $\rho_{\mu}$  controlled by a parameter  $\mu$  such that, for some  $\mu$  the function is convex and, in the limit, we obtain the original non-convex function  $\rho(\bullet)$ . We start by solving the initial convex problem and update the parameter  $\mu$ , thus increasing the non-convexity of the next problem to solve, till the original problem

is attained. The variable estimated for the  $i$ -th problem is employed as initialization for the  $(i+1)$ -th problem.

For the Tukey's biweight function in (24), the surrogate function with the control parameter  $\mu$  is given as

$$\rho_{\bar{c}}(r, \mu) = \begin{cases} \frac{r^2}{\mu \bar{c}^2} - \left(\frac{r^2}{\mu \bar{c}^2}\right)^2 + \frac{1}{3}\left(\frac{r^2}{\mu \bar{c}^2}\right)^3, & |r| \leq \sqrt{\mu} \bar{c} \\ \frac{1}{3}, & \text{otherwise} \end{cases}. \quad (26)$$

For large  $\mu$ , the function  $\rho_{\bar{c}}(r, \mu)$  is convex and returns the original function (24) when  $\mu = 1$  (see Figure (4b)). The outlier process  $\Psi_{\bar{c}}(w_i)$  in (25) for any GNC surrogate with parameter  $\mu$  is defined as

$$\Psi_{\bar{c}}(w_i, \mu) = \frac{\mu \bar{c}^2}{3} (1 - \sqrt{w_i})^2 (1 + 2\sqrt{w_i}). \quad (27)$$

### Overview of the Robust Estimation

With these tools at hand, we are now able to solve the non-convex problem (23). At each outer iteration, we update the control parameter  $\mu$  and optimize

$$\min_{\mathbf{E} \in \mathbb{E}} \sum_{i=1}^N \rho_{\bar{c}}(\epsilon_i, \mu). \quad (28)$$

with  $\rho_{\bar{c}}(\epsilon_i, \mu)$  given by (26). By the Black-Rangarajan duality, we re-formulate this surrogate problem as the joint optimization over  $\mathbf{E}$  and  $\{w_i\}_{i=1}^N$ :

$$\min_{\substack{\mathbf{E} \in \mathbb{E}, \\ w_i \in [0, 1], i=1, \dots, N}} \sum_{i=1}^N w_i \epsilon_i^2 + \Psi_{\bar{c}}(w_i, \mu). \quad (29)$$

Problem (29) is actually solved by alternating optimization. At each inner iteration, we optimize over  $\mathbf{E}$  with the previous  $\{w_i\}$  and then, we optimize over  $\{w_i\}$  with fixed  $\mathbf{E}$ . See that in the first optimization, the second term in (29) does not depend on  $\mathbf{E}$  and can be dropped. Hence, this first problem is the weighted version of the non-minimal presented in (9). The optimization over  $\{w_i\}$  with fixed  $\mathbf{E}$  can be solved in closed-form for the loss function considered here. The weight  $w_i$  is computed as:

$$w_i = \begin{cases} 0 & \frac{\epsilon_i^2}{\mu \bar{c}^2} > 1 \\ \left(1 - \frac{\epsilon_i^2}{\mu \bar{c}^2}\right)^2 & \text{otherwise} \end{cases}. \quad (30)$$

Note that  $w_i \in [0, 1]$  since  $\frac{\epsilon_i^2}{\mu \bar{c}^2} \geq 0$ .

This process, which is summarized in Algorithm (2), is repeated for decreasing values of  $\mu$  until it is equal to one. This decreasing rate is given by the parameter  $\tau_{\mu} > 1.0$ . Although Algorithm (2) only requires as input the set of correspondences, we can also provide the initialization for the local, iterative optimization algorithm that updates the variable  $\mathbf{E}$  and the initial weights associated the correspondences.

**Implementation details:** In practice, we fix the rate for  $\mu$  in  $\tau_{\mu} = 1.10$  and stop the algorithm if the difference between two consecutive cost values for *outer* iterations lies below  $10^{-6}$ . The same threshold is employed to break the inner loop, although it does not stop the estimation. We allow two

---

**Algorithm 2:** Robust Estimation of the Essential Matrix

---

**Data:** Set of correspondences  $\{(\mathbf{f}_i, \mathbf{f}'_i)\}_{i=1}^N$   
**Result:** Estimated essential matrix  $\mathbf{E}$ ; set of inliers  $\mathcal{I}$  (weights); ISVALID  $\in \{\text{True}, \text{False}\}$

```
1 Initialize  $\mu = 6000$ ;  
  // Outer iteration  
2 repeat  
  // Inner iteration  
3   repeat  
4     Update  $\mathbf{E}$  with weighted problem (9) ;  
5     Update weights  $w_i, i = 1, \dots, N$  in  
      closed-form (30) ;  
6   until convergence or max. iterations;  
7    $\mu \leftarrow \mu / \tau_\mu$  ;  
8 until  $\mu = 1$  or convergence;  
9 Set inliers:  $\mathcal{I} = \{i \mid w_i > \tau_w, i = 1, \dots, N\}$  ;  
10 if  $|\mathcal{I}| \geq N_0$  then  
11   Refine estimation (9) with set of inliers ;  
12   ISVALID = True ;  
13 else  
14   // Number of inliers is not enough  
   ISVALID = False ;
```

---

iterations for the inner loop and 500 for the outer. We define the shape parameter as  $\bar{c}^2 = 10^{-5}$  and consider as inlier any correspondence whose weight is greater than  $\tau_w = 0.9$ . In the last step, we refine the estimated essential matrix only with the set of inliers. To avoid ill-posed problems, we required that at least there exist  $N_0 = 12$  inliers. We apply our certifier to this last problem and solution defined only with the inliers.

A fast, C++ implementation of our proposal is publicly available in

<https://github.com/mergarsal/FastCertRelPose.git>. Bindings for MATLAB and PYTHON are also provided. As a by-product of our contribution, we also release a lightweight template library in

<https://github.com/mergarsal/GNCSO.git>

for the robust algorithm in (2), that currently<sup>1</sup> includes Tukey’s biweight, Welsch (Leclerc), Geman-McClure and TLS loss functions, and admits any non-minimal or minimal solver for the variable estimation step. This library also wraps around the *Optimization* library by Rosen *et al.* [52] that allows to perform local optimization on Riemannian manifold and convex spaces.

## VII. EXPERIMENTAL VALIDATION

In this last Section, we empirically showcase the utility of the proposed certifiable pipeline and the improvements presented in this work through an extensive set of experiments on both synthetic (Section (VII-B)) and real data (Section (VII-C)). Before that, we compare the proposed certifiable pipeline against the state-of-the-art certifiable approaches proposed for the RPP (Section (VII-A)). All the experiments

were performed in the same machine (PC) with: CPU intel i7-4702MQ, 2.2GHz and RAM 8 GB.

### A. Comparison against certifiable solvers

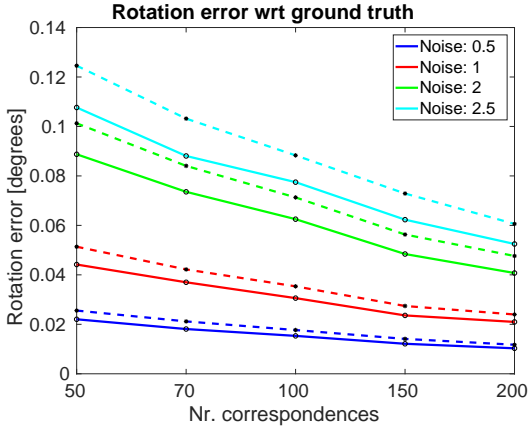
In this Section we compare the performance in terms of accuracy and computational cost of the proposed solver against the state-of-the-art certifiable approaches.

As we introduce in Section (II), certifiable solvers for the RPP exist that rely on Branch-and-Bound optimization and convex relaxations, the latter solved via Interior Point Algorithms (IPM) with off-the-shelf tools. The first set of solvers present worst-case exponential time complexity due to their exploration of the feasible set. As it has been reported in the original papers [11], [12], and recent works [15], this leads to computational times of seconds or even minutes. We will not examine further this type of solvers since the other approaches based on convex relaxations have been shown to be faster with polynomial time complexity. The complexity depends on the number of variables and constraints, which can be empirically observed when comparing, for example, [27] (40 variables and 536 constraints) and [15] (12 variables and 7 constraints). We perform a set of experiments with both solvers under a MATLAB implementation (using SDPT3 [44] as IPM), and observe that [27] takes 1-2 seconds, while [15] remains under 0.5 seconds. For the same set of experiments and under a matlab implementation, our proposal roughly takes 50 milliseconds (including variable estimation).

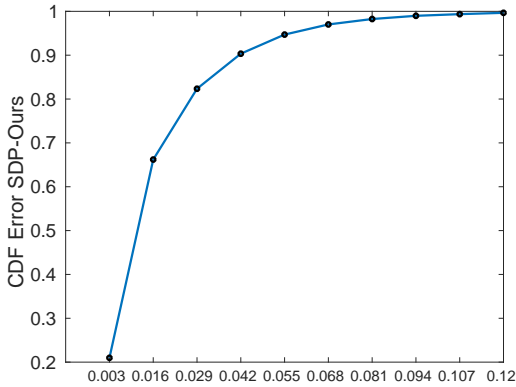
From the above discussion we can derive that the faster certifiable solver is the SDP proposed in [15]. We next perform a comparison against this SDP; we employ the released code by the author<sup>2</sup>. We perform a set of experiments on synthetic data (see Section (VII-B1) for a detailed explanation of the data generation). We observe, as it was pointed out by the author, that the relaxation does not perform always well with low number of correspondences and/or large noise. For the sake of clarity, we restrict the noise to  $\sigma = \{0.5, 1.0, 2.0, 2.5\}$  pixels and number of correspondences in  $N = \{50, 70, 100, 150, 200\}$ ; for each configuration, we generate 500 random problem instances. We measure the distance between the returned rotation matrices w.r.t. the ground truth in terms of geodesic distance. Figure (5a) shows the mean errors for each configuration of parameters. We also measure the distance between the solutions w.r.t. each other and plot the probability distribution of errors in Figure (5b). Observe that for the considered range of observations-noise, both certifiable solvers return similar solutions, while our proposal attains lower errors in rotation. This difference can be partially explained by the procedure that the SDP employs to extract the solution, that may have associated some rounding errors. While these differences are small, the computational time required by each solver does differ: the SDP requires 5 milliseconds and the proposed pipeline takes only 500 microseconds in average. That is, while the solution obtained by our proposal is similar in all occasions (if not better), reflecting in turn that the iterative solver does

<sup>1</sup>Date of this document

<sup>2</sup><https://github.com/jizhaox/npt-pose>



(a) Error in rotation (degrees) between the returned solution by our solver (solid line) and the SDP (dashed line) w.r.t. the ground truth in terms of the number of correspondences (X-axis). Legend shows the noise level for each graphic.



(b) Probability distribution of the error between the rotation returned by our solver and the one returned by the SDP for all the experiments and number of correspondences.

Fig. 5: Comparison of our solver and the SDP in [15]. Figures show the results (see captions) for the experiments with noise  $\sigma = \{0.5, 1.0, 2.0, 2.5\}$  pix and correspondences  $N = \{50, 70, 100, 150, 200\}$ .

attain the global optimum repeatedly, the certifiable pipeline is at least ten times faster than the SDP.

From a implementation point of view, we should also remark that our certification algorithm does not require specific tools, as the convex relaxations do. The proposed solver allows to estimate the variable by any means and then, it certifies the given solution. The latter requires the resolution of a linear system in six variables and the computation of two eigenvalues (one of them can be computed in closed-form), operations that any mathematical library provide with.

### B. Experiments on Synthetic data

We design four types of experiments, each of them target to show a different aspect of our proposal:

- In this first set (Section (VII-B1)) we show the performance of the current implementation with the simplification of the essential matrix manifold introduced in Section (V-A). We also prove empirically that the proposed preconditioner in Section (V-A) does reduce the number of iterations of the RTR solver.
- In this second set (Section (VII-B2)) we compare the proposed certifiable pipeline with state-of-the-art methods [11] in both performance and computation time.
- In this third set (Section (VII-B3)) we compare the performance of Bundle-adjustment (minimization of re-projection error) when initialized with minimal solvers and our proposal.
- In this fourth set (Section (VII-B4)) we introduce outliers and compare the performance of our robust pipeline (Section (VI)) against minimal solvers embedded into a RANSAC framework, which can be considered as the most common approach to robustification.

We employ the same procedure to generate the random data for all our synthetic experiments, which is the same procedure used in previous works [13], [27]. We summarize it here for completeness: We place the first camera frame at the origin (identity orientation and zero translation) and generate a set of random 3D points within a frustum with depth ranging from one to eight meters measured from the first camera frame and inside its Field of View (FoV). Then, we generate a random pose for the second camera whose translation magnitude is bounded above by  $\|t\|_{\max}$ . We also enforce that all the 3D points lie within the second camera's FoV. We create the correspondences as unit bearing vectors and add noise by assuming a spherical camera, computing the tangential plane at each bearing vector (point on the sphere) and introducing a random error sampled from the standard uniform distribution, considering a focal length of 800 pixels for both cameras.

1) *Performance of the current implementation without outliers:* In order to showcase the performance of our proposal and the computational improvements with respect to our previous work [13], we design three batch of experiments:

**Influence of Parameters:** We show first the performance of the proposed certifiable pipeline for instances of the RPP with different parameters and initialized with the 8-PT algorithm. We use the following default parameters and change one of them in each batch of experiments: FOV to 100 degrees, translation parallax  $\|t\|_{\max} = 2.0\text{m}$ , focal length of  $f = 800$  pix and noise level  $0.5$  pix. We consider four level of noise  $\sigma = \{0.1, 0.5, 1.0, 2.5\}$  pix, four values for the maximum parallax  $\|t\|_2 = \{1.0, 1.5, 2.5, 4.0\}$  m, four FOV angles  $\text{FOV} \in \{70, 90, 120, 150\}$  degrees (focal length fixed) and four focal lengths  $f \in \{300, 600, 1000, 1200\}$  pix (image size fixed). For each configuration of parameters, we generate random problem instances as explained above with number of correspondences in  $N \in \{8, 9, 10, 11, 12, 13, 14, 15, 40, 100, 150, 200\}$ . Further, for each combination of parameter/number of correspondences, we generate 500 random instances.

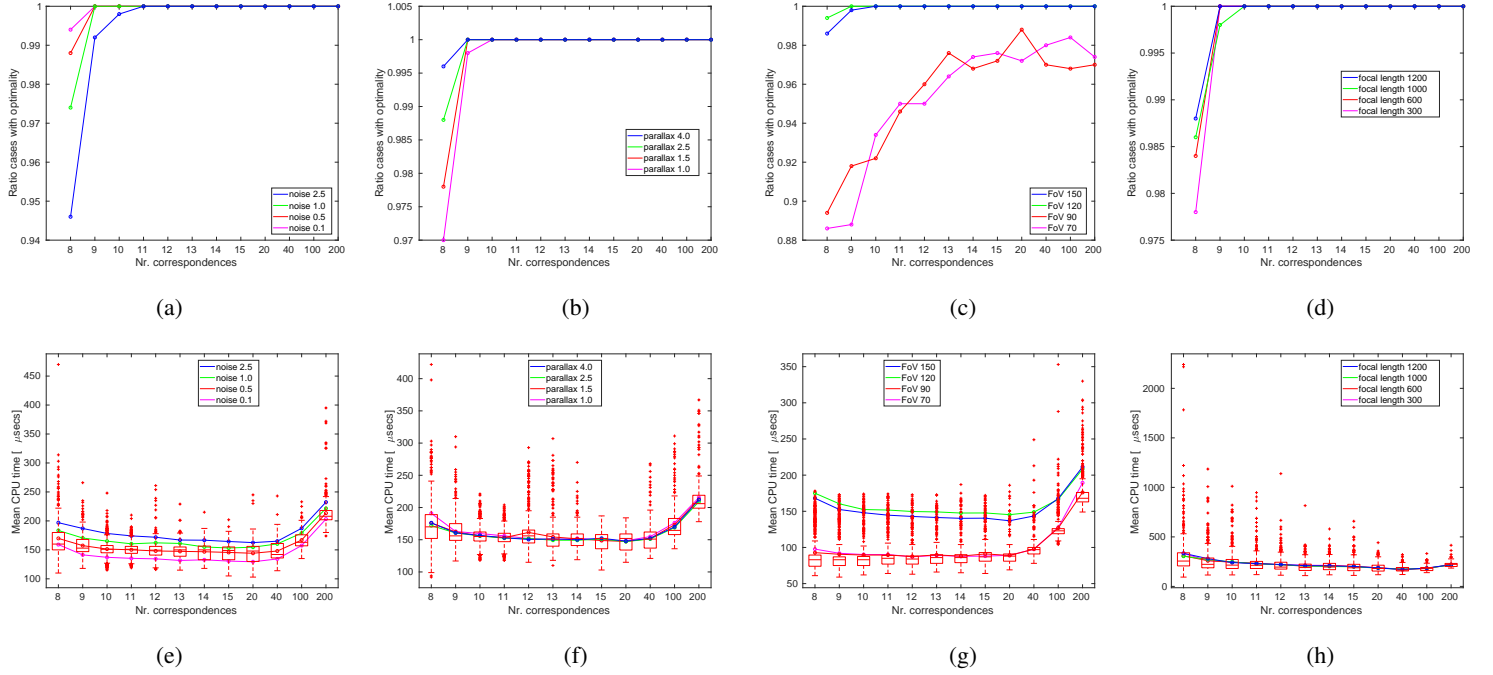


Fig. 6: Percentage of cases (first row) in which we could certify the optimality of the solution (note the difference for the Y-axis scale between figures); and averaged computation time (second row, solid line) in  $\mu\text{secs}$  required by the whole proposed pipeline. We include (second row) the boxplots with the results for noise  $0.5 \text{ pix}$ , maximum parallax  $1.5 \text{ m}$ , FOV  $90$  degrees and focal length  $f = 600 \text{ pix}$ .

Figures (6a),(6b),(6c) and (6d) show the percentage of cases with *certified* optimal solutions (Algorithm (1)) for the experiments with different level of noise, parallax, FOV and focal length, respectively. We plot the averaged computation time in  $\mu\text{secs}$  for the three batches of experiments in Figures (6e),(6f), (6g) and (6h). We also include the results as boxplots<sup>3</sup> for the experiments with noise  $0.5 \text{ pix}$ , maximum translation magnitude of  $1.5 \text{ m}$ , FOV  $90$  degrees and focal length  $f = 600 \text{ pix}$  (same color than the mean values).

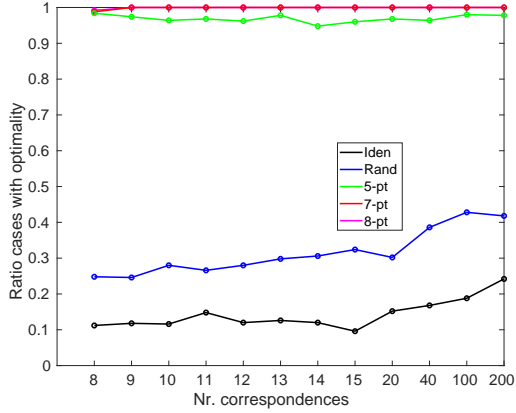
The simplified characterization of the essential matrix manifold chosen for this implementation (Section (V-A)) does not seem to affect the overall performance of the proposed certifiable pipeline, as it is reflected by the high percentage of cases with certified optimal solutions. As expected, the cases with low number of correspondences (up to  $9 - 11$ ) present the worst behavior, although the percentage of optimal solutions goes up to  $94\%$ . From scenes with more than  $11$  correspondences, we obtain  $100\%$  of certified cases for all the different parameters (noise, translation and FOV), except those with narrow FOV ( $70 - 90$  degrees). For the latter, we observe that with more than  $12$  correspondences, we are able to certify as optimal more than  $90\%$  of the solutions. Further, we see that the averaged computation time for all the instances

is under  $250 \mu\text{secs}$ , even in challenging instances with high noise, narrow FOV and small focal length (a large signal-to-noise ratio).

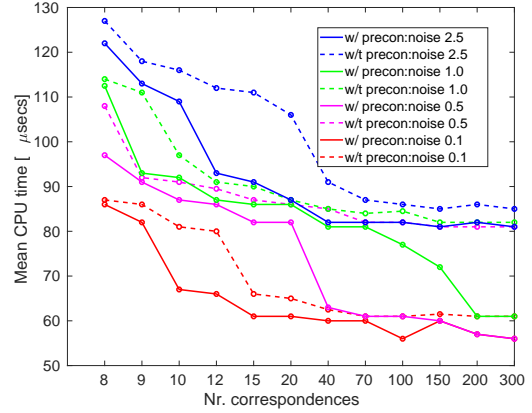
**Influence of Initialization:** Here we show the influence of the initialization on the performance of the proposed pipeline. We generate random instances with the default parameters given above and initialize the pipeline with the trivial identity matrix (IDEN), a random matrix (RAND), the estimation obtained with the 5-point algorithm (5-PT) [19], with the 7-point algorithm (7-PT) and the 8-pt algorithm (8-PT). We generate 500 problem instances.

Figure (7a) depicts the percentage of cases with certified optimal solution. We see that the ratio of optimal solutions from the 5-PT, 7-PT and 8-PT are similar ( $> 90\%$ ), while being slightly higher for the last two initializations. On the other hand, the solutions obtained with the random and identity matrices tend to percentages below  $40\%$  and  $30\%$ , respectively. This last result reflects a considerable difference with respect to [13], in which we obtain an increasing percentage of optimal solutions (up to  $95\%$ ) with the number of correspondences for these initializations. The simplification of the essential matrix manifold in this work, while it does not seem to affect the refinements initialized with the 5-PT, 7-PT or 8-PT algorithms, it hinders the optimizations with poor initializations. In practice, however, one should never initialize the algorithm with these matrices; even a “bad“ estimation (e.g. high noise and 8-PT) is shown to attain the global

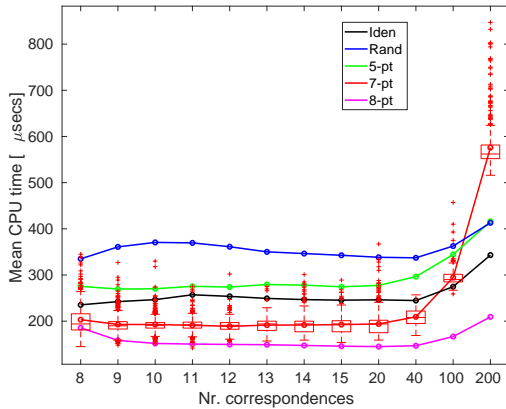
<sup>3</sup>All the boxplots that appear in this manuscript follow the same (matlab) format: central mark indicates median, the bottom and top edges indicate the 25th and 75th percentile, respectively and the whiskers denote the data that is not considered as outlier. The latter are plotted individually with the ‘+’ symbol.



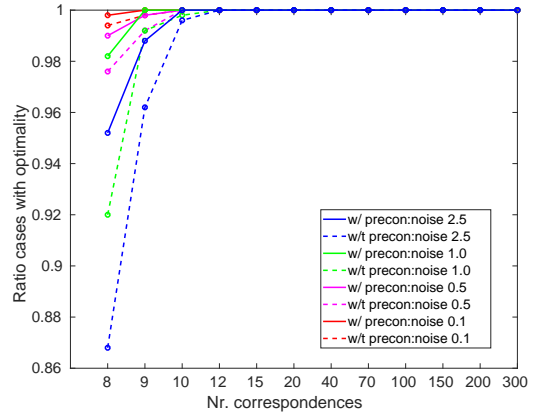
(a)



(a)



(b)



(b)

Fig. 7: Percentage of cases ((7a)) in which we certify the solution as optimal (the graphics for 7-PT and 8-PT overlap); and averaged computation time (solid line, (7b)) required by the certifiable pipeline. We include as boxplot the time for the optimizations initialized with the 7-PT (boxplot, (7b)). Observe that the instability of the 5-PT may affect the performance of the iterative solver, which is reflected by the percentage of optimal solutions not being 100% in (7a). Figures reported the experiments with default parameters (noise 0.5 pix and focal length 800 pix).

optimum with high probability. In terms of computational time, we observe that for all the cases the complete certifiable pipeline takes less than  $400\mu\text{secs}$  to return a solution.

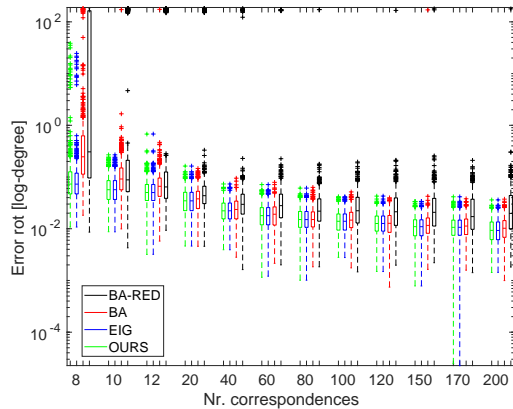
**Influence of the Preconditioner** The last batch of experiments within this set is devoted to the proposed preconditioner in Section (V-A). We generate random instances of the RPP with the default parameters and varying level of noise and number of correspondences. The proposed certifiable pipeline is initialized with the 8-PT estimation and the optimization is performed with and without the preconditioner.

Figure (8a) depicts the averaged computation time in mi-

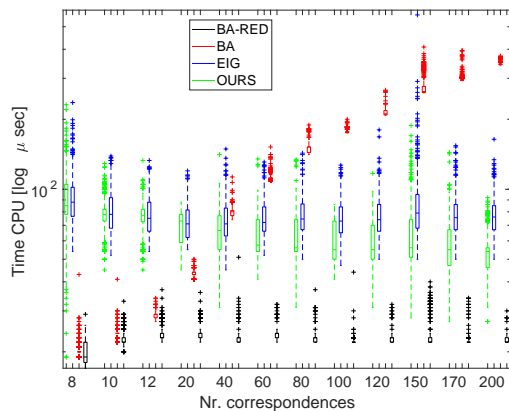
Fig. 8: Averaged computation time (8a) required by the certifiable pipeline with (solid line) and without preconditioner (dashed line); and percentage of cases (8b) in which we certify the solution as optimal with (solid line) and without (dashed line) preconditioner for different levels of noise.

croseconds required by our proposal to produce a solution for each level of noise and number of correspondences. In terms of computation time, the main advantage of using this preconditioner is seen for those problems with a large number of correspondences. It turns out, however, that its effect goes beyond its main purpose and it is also reflected in the percentage of optimal solutions, as it is shown in Figure (8b) for those problems with less than 12 correspondences.

**Computational cost:** Here we break down the computational cost of the certifiable pipeline in Section (V) by considering its three main steps: (1) initialization; (2) refinement; and (3) certification. The first stage depends on which solver is used for the initialization; for the 8-PT we measure less than  $60\mu\text{secs}$  in average, considering also the data matrix  $C$  generation and the computation of the preconditioner. The refinement stage depends on the quality of the initial guess,



(a)



(b)

Fig. 9: Error in rotation in (log) degrees (9a); and computation time (9b) in (log)  $\mu\text{secs}$  for our proposed pipeline OURS, the eigen-formulation in [11] EIG, the standard non-linear optimization BA; and its reduced version with only 10 points BARED.

which a priori cannot be measured. We observe, however, that with the 8-PT as initialization, this stage takes less than 100  $\mu\text{secs}$  despite noise, number of correspondences and FOV. Last, we consider the two main steps for the certification: (a) computing the dual candidates (solving equation (7)); and (b) checking the spectral condition of the blocks of the Hessian  $M^e(\hat{\lambda}), M^t(\hat{\lambda})$ . Both steps take an average of 40  $\mu\text{secs}$  for relaxation. In practice, two certifiers are able to certify most of the solutions. Considering this case, the computational time of the certification stage rise to 150  $\mu\text{secs}$ . Therefore, the computational cost of the complete certifiable pipeline tends to remain below 300  $\mu\text{secs}$ .

2) *Comparison with state-of-the-art estimators without outliers*: In these experiments, we compare the proposed certifiable pipeline with the state-of-the-art non-minimal methods. We denote by EIG the estimator proposed in [11], by BA the

non-linear iterative minimization of the reprojection error and by BARED the same non-linear optimization, but restricted to ten random correspondences. We employ the implementation for these methods as it is provided by the computer vision library OPENGV [56]. Recall that none of these methods is able to certify optimality.

We generate random instances with the default parameters given above and for each combination, we generate 500 instances. In this case, the number of correspondences are  $N = \{8, 10, 12, 20, 40, 60, 80, 100, 120, 150, 170, 200\}$ . We initialize all the algorithms with the same point  $(\mathbf{R}, \mathbf{t})$  obtained from the 8-PT.

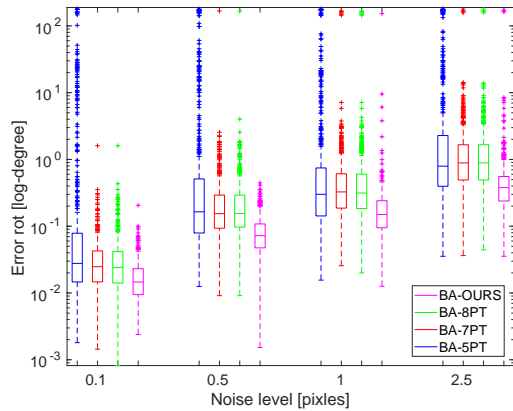
Figure (9a) shows the rotation error in logarithmic scale, measured as the geodesic distance between the estimated rotation and the ground truth. Note that EIG and OURS have similar error, of the order of BA. Figure (9b) depicts the computation time required by the optimization stage in log-microseconds for the different methods.

While the error attained by OURS, EIG and BA are similar for problem instances with  $N \geq 20$ , Figure (9b) shows that OURS required less time to achieve the same solution than the other two. Since BARED only employs 10 correspondences, it requires less CPU time although attains the largest error among all the methods.

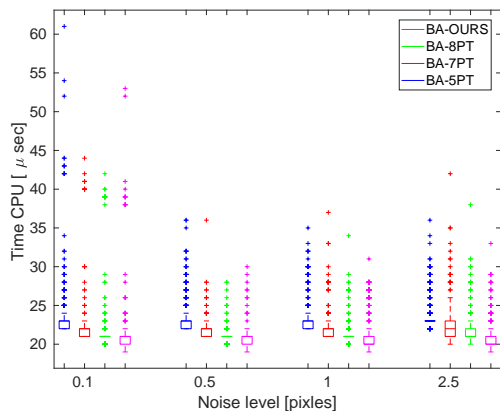
3) *Influence in Bundle-Adjustment*: In this set of experiments we compare the performance, both in error and time, of the non-linear BA initialized with the previous minimal solvers and our proposal, since these minimal solvers are usually employed as initialization. We compare the 5-PT (denoted as BA-5PT), the 7-PT (BA-7PT) and the 8-PT (BA-8PT) with our proposal (BA-OURS). We generate random problem instances with the default parameters and vary the level of noise. We fix the number of correspondences in 9 and feed each method with their minimal number of points (our approach is executed with the 9 points). The multiple solutions are disambiguate with the remaining points. We create 500 random problem instances for each level of noise.

Figure (10a) depicts the error in rotation (log-degrees) w.r.t. the ground truth for each solution returned by BA with the different initialization. While the 7-PT and 8-PT perform similarly, OURS attains the lowest error despite the noise. In terms of time, Figure (10b) shows the computation time required by BA (in log  $\mu\text{secs}$ ) for all the algorithms. Similarly, 7-PT and 8-PT require comparable times, while OURS is faster. The computational times reported in this set of experiments did not include the initialization stage, only the time required by the BA to converge. We observe that in general our proposed pipeline increase the accuracy of BA and reduce the time to convergence.

4) *Performance of the robust certifiable pipeline and comparison with state-of-the-art methods with outliers*: This last set of experiments on synthetic data is aimed to show the resiliency of our robust proposed pipeline (Algorithm (2)) in Section (VI) against outliers: we apply the algorithm with the Tukey's biweight (TUKEY) and Geman-McClure (GM)



(a)



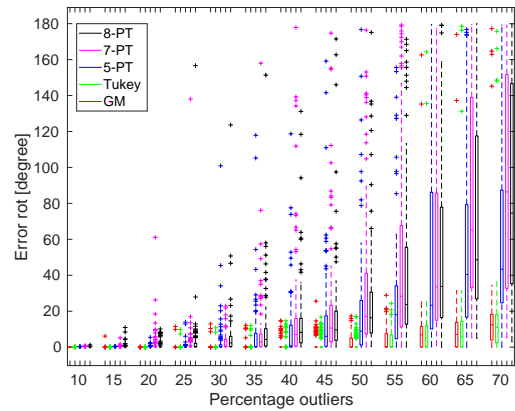
(b)

Fig. 10: Error in rotation in (log) degrees (9a); and computation time (9b) in  $\mu secs$  for Bundle-adjustment initialized with the 5-PT , the 7-PT , the 8-PT and our proposed pipeline OURS.

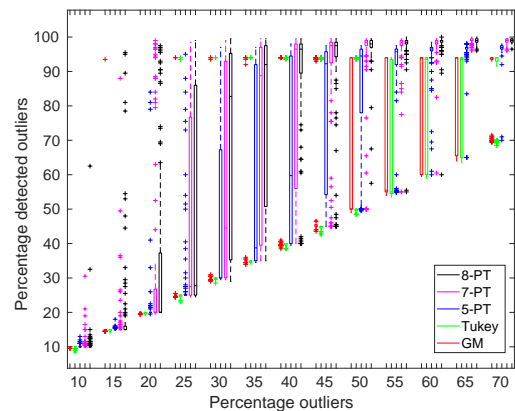
loss functions. We also compare it with the non-iterative solvers, *i.e.* 5-PT , 7-PT and 8-PT , embedded in a RANSAC framework.

We generate random problem instances with the default parameters. In order to help the methods, we employ 200 points and increase the FOV up to 150 degrees. We introduce outliers by substituting the correspondence associated with the second frame by a random (unitary) vector. We increase the percentage of outliers with a fixed step of 5 % and for each of them, we generate 100 random problem instances.

Figure (11a) shows the error in rotation (degrees) for each compared method. While the approaches based in RANSAC fail with 30% of outliers (the one with 5-PT performs better than 7-PT and 8-PT though), the proposed approach is able to return a solution with low error up to 50% of bad correspondences. Further, up to 70% of outliers (high ratio of outliers), the error attained by our proposal remains below



(a)



(b)

Fig. 11: Error in rotation in degrees (11a); and percentage of detected inliers (11b) for the different robust methods compared.

40 degrees (with a mean value of 11 degrees), while the RANSAC paradigms go up to 180 degrees (minimum mean value is 62 degrees).

Figure (11b) shows the percentage of detected outliers (Y-axis) for each method as a function of the percentage of generated outliers (X-axis). These results provide an explanation on the errors depicted in (11a): when the number of detected inliers decrease (see *e.g.* our method with more than 55% outliers), the solution returned attain highest errors.

**Computational cost:** Last, we summarize here the computational cost of Algorithm (2) and compare it against the average values for the RANSAC paradigms. The proposed algorithm requires 60 – 80 outer iterations and 3 – 4 inner iterations for any rate of outliers (except for 0% of outliers, case in which it only runs one iteration) and the set of parameters employed. The relative pose estimation is the slowest step in the Algorithm, taking an average of 300  $\mu secs$ . In total, the robust pipeline requires 20–30 *msecs* to estimate

a solution. On the other hand, RANSAC-based schemes take an average of  $1 - 2$  *msecs*, being slower when the 5-PT is used as minimal solver and/or when the number of outliers is large.

### C. Experiments on Real Data

To conclude this experimental validation, we evaluate our robust certifiable proposal (Algorithm (2)) on real data. To cover a wide regimen of real scenarios we select three available datasets, with both indoor and outdoor scenes, ground truth and intrinsic calibration parameters: ETH3D [57], TUM [58] and CVPR08 [59]. The sequences employed here are listed in the *Online Resource* (Section (D)). For all of them, we generate the correspondences by extracting and matching 100 SURF features [60]. We compute the equivalent unitary bearing vectors by applying the pin-hole camera model with the provided intrinsic parameters for each frame. For each pair of images, we run the minimal solvers (5-PT, 7-PT and 8-PT) embedded into a RANSAC scheme (RANSAC-5PT, RANSAC-7PT, RANSAC-8PT) and our proposed robust pipeline (OURS).

Figure (12) depicts the error in rotation (in terms of geodesic distance) for all the tested methods. For our proposal, we also include the error for those solutions that were certified as optimal (OURS-CERT). We observe how our robust pipeline achieves better results in general than the most employed robust solvers. See also how the optimal solutions tend to attain the lower errors. However, an optimal solution does not guarantee that all the outliers are discarded: the certification is performed for a concrete problem instance and solution. Last, the percentage of certified optimal solutions for each dataset were: ETH3D 98.5379%, TUM 82.6201% and CVPR08 99.0741%. We break down the percentage for each sequence and provide the error in rotation in the *Online Resource* (E).

## VIII. CONCLUSIONS AND FUTURE WORK

In this work we extended our previous work in [13] and proposed an efficient and robust certifiable relative pose estimation. We stated the RPP as an optimization problem that minimizes the squared, normalized epipolar error over the set of normalized essential matrices. We provided a family of closed-form dual candidates derived from the six different relaxations of the set of essential matrices. These optimality certifiers were incorporated as final stage of an efficient, certifiable essential matrix estimation pipeline that first estimates a solution to the RPP by iteratively refining on the product space of 3D rotations and 2-sphere an initial guess for this problem. We derived the Euclidean quadratic model of the RPP required by the iterative solver. To speed up the convergence of the solver, we proposed a suitable preconditioner that also increased the number of certified solutions. Our proposal was proved through extensive experiments on synthetic data to be more accurate than the state-of-the-art closed-form methods, and faster than the iterative solvers. We showed that the gold standard approach for the RPP, the 2-view Bundle-adjustment,

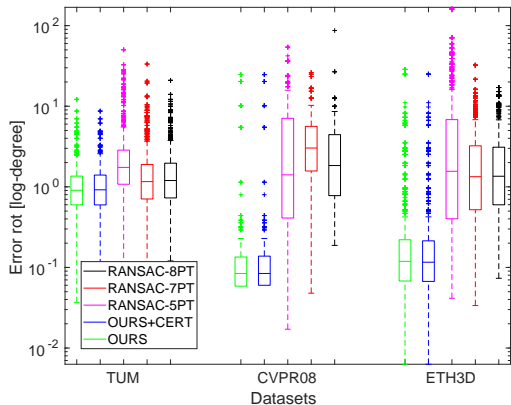


Fig. 12: Error in rotation (log scale) for the different datasets in which we evaluate the performance of our robust proposal in Algorithm (2), denoted as OURS and the minimal solvers embedded into RANSAC paradigms: 5-PT (RANSAC-5PT), 7-PT (RANSAC-7PT) and 8-PT (RANSAC-8PT). We also show the error in rotation for those cases in which we could certify optimality (OURS-CERT).

converged faster and attained a lower error when initialized with the output of our algorithm in comparison with other suitable initializations.

We integrated our certifiable approach into the robust paradigm formed by the combination of Graduated Non-convexity and the Black-Rangarajan duality between robust and line process. Our robust pipeline was proved to be less sensible to high rates of outliers (up to 50%) in comparison with the common RANSAC approaches with the closed-form solvers. Last, our evaluation on real data confirmed the observations derived from the previous experiments, and more than 80% of optimal solutions were certified for the three datasets considered. We made the code publicly available as an additional contribution, and also provided a generic library that implemented the robust paradigm here defined that was not restricted to the RPP.

As future work, we consider the extension of our certifiable stage to consider other minimal characterizations of the set of essential matrices. Further enhancements on the verification algorithm are being considered for implementation.

### ACKNOWLEDGEMENTS

This work was supported by the grant program FPU18/01526 funded by the Spanish Government and the research project WISER (DPI2017-84827-R).

### REFERENCES

- [1] Richard Hartley and Andrew Zisserman. *Multiple view geometry in computer vision*. Cambridge university press, 2003.
- [2] Ruben Gomez-Ojeda and Javier Gonzalez-Jimenez. Robust stereo visual odometry through a probabilistic combination of points and line segments. In *2016 IEEE International Conference on Robotics and Automation (ICRA)*, pages 2521–2526. IEEE, 2016.

- [3] David Nistér, Oleg Naroditsky, and James Bergen. Visual odometry. In *Proceedings of the 2004 IEEE Computer Society Conference on Computer Vision and Pattern Recognition, 2004. CVPR 2004.*, volume 1, pages I–I. Ieee, 2004.
- [4] Davide Scaramuzza and Friedrich Fraundorfer. Visual odometry [tutorial]. *IEEE robotics & automation magazine*, 18(4):80–92, 2011.
- [5] Takafumi Taketomi, Hideaki Uchiyama, and Sei Ikeda. Visual slam algorithms: a survey from 2010 to 2016. *IPSSJ Transactions on Computer Vision and Applications*, 9(1):16, 2017.
- [6] Christian Kerl, Jürgen Sturm, and Daniel Cremers. Dense visual slam for rgb-d cameras. In *2013 IEEE/RSJ International Conference on Intelligent Robots and Systems*, pages 2100–2106. IEEE, 2013.
- [7] Ruben Gomez-Ojeda, Francisco-Angel Moreno, David Zuñiga-Noël, Davide Scaramuzza, and Javier Gonzalez-Jimenez. Pl-slam: A stereo slam system through the combination of points and line segments. *IEEE Transactions on Robotics*, 35(3):734–746, 2019.
- [8] Johannes L Schonberger and Jan-Michael Frahm. Structure-from-motion revisited. In *Proceedings of the IEEE Conference on Computer Vision and Pattern Recognition*, pages 4104–4113, 2016.
- [9] Changchang Wu. Towards linear-time incremental structure from motion. In *2013 International Conference on 3D Vision-3DV 2013*, pages 127–134. IEEE, 2013.
- [10] Matthew J Westoby, James Brasington, Niel F Glasser, Michael J Hambrey, and Jennifer M Reynolds. ‘structure-from-motion’ photogrammetry: A low-cost, effective tool for geoscience applications. *Geomorphology*, 179:300–314, 2012.
- [11] Laurent Kneip and Simon Lynen. Direct optimization of frame-to-frame rotation. In *Proceedings of the IEEE International Conference on Computer Vision*, pages 2352–2359, 2013.
- [12] Richard I Hartley and Fredrik Kahl. Global optimization through searching rotation space and optimal estimation of the essential matrix. In *2007 IEEE 11th International Conference on Computer Vision*, pages 1–8. IEEE, 2007.
- [13] Mercedes Garcia-Salguero, Jesus Briales, and Javier Gonzalez-Jimenez. Certifiable relative pose estimation. *Image and Vision Computing*, 109:104142, 2021.
- [14] Minas E Spetsakis and Yiannis Aloimonos. Optimal visual motion estimation: A note. *IEEE Transactions on Pattern Analysis & Machine Intelligence*, (9):959–964, 1992.
- [15] Ji Zhao. An efficient solution to non-minimal case essential matrix estimation. *IEEE Transactions on Pattern Analysis and Machine Intelligence*, 2020.
- [16] Yi Ma, Jana Koščeká, and Shankar Sastry. Optimization criteria and geometric algorithms for motion and structure estimation. *International Journal of Computer Vision*, 44(3):219–249, 2001.
- [17] Uwe Helmke, Knut Hüper, Pei Yean Lee, and John Moore. Essential matrix estimation using gauss-newton iterations on a manifold. *International Journal of Computer Vision*, 74(2):117–136, 2007.
- [18] Peter Decker, Dietrich Paulus, and Tobias Feldmann. Dealing with degeneracy in essential matrix estimation. In *2008 15th IEEE International Conference on Image Processing*, pages 1964–1967. IEEE, 2008.
- [19] David Nistér. An efficient solution to the five-point relative pose problem. *IEEE transactions on pattern analysis and machine intelligence*, 26(6):756–770, 2004.
- [20] Henrik Stewenius, Christopher Engels, and David Nistér. Recent developments on direct relative orientation. *ISPRS Journal of Photogrammetry and Remote Sensing*, 60(4):284–294, 2006.
- [21] Vincent Lui and Tom Drummond. An iterative 5-pt algorithm for fast and robust essential matrix estimation. In *BMVC*, 2013.
- [22] Tom Botterill, Steven Mills, and Richard Green. Refining essential matrix estimates from ransac. In *Proceedings Image and Vision Computing New Zealand*, pages 1–6, 2011.
- [23] Olivier D Faugeras and Steve Maybank. Motion from point matches: multiplicity of solutions. *International Journal of Computer Vision*, 4(3):225–246, 1990.
- [24] Yi Ma, Stefano Soatto, Jana Kosecka, and S Shankar Sastry. *An invitation to 3-d vision: from images to geometric models*, volume 26. Springer Science & Business Media, 2012.
- [25] Seong Hun Lee and Javier Civera. Geometric interpretations of the normalized epipolar error. *arXiv preprint arXiv:2008.01254*, 2020.
- [26] Roberto Tron and Kostas Daniilidis. The space of essential matrices as a riemannian quotient manifold. *SIAM Journal on Imaging Sciences*, 10(3):1416–1445, 2017.
- [27] Jesus Briales, Laurent Kneip, and Javier Gonzalez-Jimenez. A certifiably globally optimal solution to the non-minimal relative pose problem. In *Proceedings of the IEEE Conference on Computer Vision and Pattern Recognition*, pages 145–154, 2018.
- [28] Afonso S Bandeira. A note on probably certifiably correct algorithms. *Comptes Rendus Mathématique*, 354(3):329–333, 2016.
- [29] Anders Eriksson, Carl Olsson, Fredrik Kahl, and Tat-Jun Chin. Rotation averaging and strong duality. In *Proceedings of the IEEE Conference on Computer Vision and Pattern Recognition*, pages 127–135, 2018.
- [30] José Pedro Iglesias, Carl Olsson, and Fredrik Kahl. Global optimality for point set registration using semidefinite programming. In *Proceedings of the IEEE/CVF Conference on Computer Vision and Pattern Recognition*, pages 8287–8295, 2020.
- [31] Jesus Briales and Javier Gonzalez-Jimenez. Convex global 3d registration with lagrangian duality. In *Proceedings of the IEEE Conference on Computer Vision and Pattern Recognition*, pages 4960–4969, 2017.
- [32] Jesus Briales and Javier Gonzalez-Jimenez. Fast global optimality verification in 3d slam. In *2016 IEEE/RSJ International Conference on Intelligent Robots and Systems (IROS)*, pages 4630–4636. IEEE, 2016.
- [33] Luca Carlone, David M Rosen, Giuseppe Calafiore, John J Leonard, and Frank Dellaert. Lagrangian duality in 3d slam: Verification techniques and optimal solutions. In *2015 IEEE/RSJ International Conference on Intelligent Robots and Systems (IROS)*, pages 125–132. IEEE, 2015.
- [34] Luca Carlone and Frank Dellaert. Duality-based verification techniques for 2d slam. In *2015 IEEE international conference on robotics and automation (ICRA)*, pages 4589–4596. IEEE, 2015.
- [35] Rahul Raguram, Jan-Michael Frahm, and Marc Pollefeys. A comparative analysis of ransac techniques leading to adaptive real-time random sample consensus. volume 5303, pages 500–513, 10 2008.
- [36] Andrew Blake and Andrew Zisserman. *Visual reconstruction*. MIT press, 1987.
- [37] Michael J Black and Anand Rangarajan. On the unification of line processes, outlier rejection, and robust statistics with applications in early vision. *International journal of computer vision*, 19(1):57–91, 1996.
- [38] Heng Yang, Jingnan Shi, and Luca Carlone. Teaser: Fast and certifiable point cloud registration. *arXiv preprint arXiv:2001.07715*, 2020.
- [39] Heng Yang, Pasquale Antonante, Vasileios Tzoumas, and Luca Carlone. Graduated non-convexity for robust spatial perception: From non-minimal solvers to global outlier rejection. *IEEE Robotics and Automation Letters*, 5(2):1127–1134, 2020.
- [40] Zuzana Kukelova and Tomas Pajdla. Two minimal problems for cameras with radial distortion. In *2007 IEEE 11th International Conference on Computer Vision*, pages 1–8. IEEE, 2007.
- [41] Zuzana Kukelova, Martin Bujnak, and Tomas Pajdla. Polynomial eigenvalue solutions to the 5-pt and 6-pt relative pose problems. In *BMVC*, volume 2, page 2008, 2008.
- [42] P-A Absil, Robert Mahony, and Rodolphe Sepulchre. *Optimization algorithms on matrix manifolds*. Princeton University Press, 2009.
- [43] Jiaolong Yang, Hongdong Li, and Yunde Jia. Optimal essential matrix estimation via inlier-set maximization. In *European Conference on Computer Vision*, pages 111–126. Springer, 2014.
- [44] Kim-Chuan Toh, Michael J Todd, and Reha H Tütüncü. Sdpt3—a matlab software package for semidefinite programming, version 1.3. *Optimization methods and software*, 11(1-4):545–581, 1999.
- [45] Jos F Sturm. Using sedumi 1.02, a matlab toolbox for optimization over symmetric cones. *Optimization methods and software*, 11(1-4):625–653, 1999.
- [46] Stephen Boyd and Lieven Vandenberghe. *Convex optimization*. Cambridge university press, 2004.
- [47] Ji Zhao, Wanting Xu, and Laurent Kneip. A certifiably globally optimal solution to generalized essential matrix estimation. In *Proceedings of the IEEE/CVF Conference on Computer Vision and Pattern Recognition*, pages 12034–12043, 2020.
- [48] Chris Aholt, Sameer Agarwal, and Rekha Thomas. A qqcp approach to triangulation. In *European Conference on Computer Vision*, pages 654–667. Springer, 2012.
- [49] Heng Yang and Luca Carlone. A quaternion-based certifiably optimal solution to the wahba problem with outliers. In *Proceedings of the IEEE International Conference on Computer Vision*, pages 1665–1674, 2019.
- [50] Matthew Giamou, Ziye Ma, Valentin Peretroukhin, and Jonathan Kelly. Certifiably globally optimal extrinsic calibration from per-sensor ego-motion. *IEEE Robotics and Automation Letters*, 4(2):367–374, 2019.

- [51] Jesus Briales and Javier Gonzalez-Jimenez. Cartan-sync: Fast and global se (d)-synchronization. *IEEE Robotics and Automation Letters*, 2(4):2127–2134, 2017.
- [52] David M Rosen, Luca Carlone, Afonso S Bandeira, and John J Leonard. Se-sync: A certifiably correct algorithm for synchronization over the special euclidean group. *The International Journal of Robotics Research*, 38(2-3):95–125, 2019.
- [53] H Christopher Longuet-Higgins. A computer algorithm for reconstructing a scene from two projections. *Nature*, 293(5828):133–135, 1981.
- [54] N. Boumal, B. Mishra, P.-A. Absil, and R. Sepulchre. Manopt, a Matlab toolbox for optimization on manifolds. *Journal of Machine Learning Research*, 15:1455–1459, 2014.
- [55] Gijs Dubbelman, Leo Dorst, and Henk Pijls. Manifold statistics for essential matrices. In *European Conference on Computer Vision*, pages 531–544. Springer, 2012.
- [56] Laurent Kneip and Paul Furgale. Opengv: A unified and generalized approach to real-time calibrated geometric vision. In *2014 IEEE International Conference on Robotics and Automation (ICRA)*, pages 1–8. IEEE, 2014.
- [57] Thomas Schops, Johannes L Schonberger, Silvano Galliani, Torsten Sattler, Konrad Schindler, Marc Pollefeys, and Andreas Geiger. A multi-view stereo benchmark with high-resolution images and multi-camera videos. In *Proceedings of the IEEE Conference on Computer Vision and Pattern Recognition*, pages 3260–3269, 2017.
- [58] J. Sturm, N. Engelhard, F. Endres, W. Burgard, and D. Cremers. A benchmark for the evaluation of rgb-d slam systems. In *Proc. of the International Conference on Intelligent Robot Systems (IROS)*, Oct. 2012.
- [59] Christoph Strecha, Wolfgang Von Hansen, Luc Van Gool, Pascal Fua, and Ulrich Thoennessen. On benchmarking camera calibration and multi-view stereo for high resolution imagery. In *2008 IEEE Conference on Computer Vision and Pattern Recognition*, pages 1–8. Ieee, 2008.
- [60] Herbert Bay, Tinne Tuytelaars, and Luc Van Gool. Surf: Speeded up robust features. In *European conference on computer vision*, pages 404–417. Springer, 2006.

APPENDIX A  
JACOBIAN OF THE CONSTRAINTS MATRICES

In this Section we provide the Jacobian of the constraints, denoted by  $\mathbf{J}(\mathbf{x})$  for the family of relaxations considered in this work. Each relaxation has an associated  $12 \times 6$  Jacobian matrix of full rank. The explicit form of the Jacobian associated with the  $i$ -th relaxation is obtained by dropping the  $(i + 1)$ -th column of the matrix

$$\tilde{\mathbf{J}}(\mathbf{x}) = \begin{pmatrix} 0 & \mathbf{e}_1 & \mathbf{e}_7/2 & 0 & 0 & 0 & \mathbf{e}_4/2 \\ 0 & 0 & 0 & \mathbf{e}_4 & \mathbf{e}_7/2 & 0 & \mathbf{e}_1/2 \\ 0 & 0 & \mathbf{e}_1/2 & 0 & \mathbf{e}_4/2 & \mathbf{e}_7 & 0 \\ 0 & \mathbf{e}_2 & \mathbf{e}_8/2 & 0 & 0 & 0 & \mathbf{e}_5/2 \\ 0 & 0 & 0 & \mathbf{e}_5 & \mathbf{e}_8/2 & 0 & \mathbf{e}_2/2 \\ 0 & 0 & \mathbf{e}_2/2 & 0 & \mathbf{e}_5/2 & \mathbf{e}_8 & 0 \\ 0 & \mathbf{e}_3 & \mathbf{e}_9/2 & 0 & 0 & 0 & \mathbf{e}_6/2 \\ 0 & 0 & 0 & \mathbf{e}_6 & \mathbf{e}_9/2 & 0 & \mathbf{e}_3/2 \\ 0 & 0 & \mathbf{e}_3/2 & 0 & \mathbf{e}_6/2 & \mathbf{e}_9 & 0 \\ \mathbf{t}_1 & 0 & \mathbf{t}_3/2 & -\mathbf{t}_1 & 0 & -\mathbf{t}_1 & \mathbf{t}_2/2 \\ \mathbf{t}_2 & -\mathbf{t}_2 & 0 & 0 & \mathbf{t}_3/2 & -\mathbf{t}_2 & \mathbf{t}_1/2 \\ \mathbf{t}_3 & -\mathbf{t}_3 & \mathbf{t}_1/2 & -\mathbf{t}_3 & \mathbf{t}_2/2 & 0 & 0 \end{pmatrix} \quad (31)$$

Recall that the  $i$ -th relaxation is obtained by dropping the  $(i + 1)$ -th constraint in  $\mathbb{E}$ .

For the relaxation chosen in the main manuscript (we drop  $h_7 \equiv \mathbf{e}_1^T \mathbf{e}_2 + \mathbf{t}_1 \mathbf{t}_2 = 0$ ), the Jacobian that appears in Equation (7) has the form:

$$\mathbf{J}(\mathbf{x}) \doteq \begin{pmatrix} 0 & \mathbf{e}_1 & \mathbf{e}_7/2 & 0 & 0 & 0 \\ 0 & 0 & 0 & \mathbf{e}_4 & \mathbf{e}_7/2 & 0 \\ 0 & 0 & \mathbf{e}_1/2 & 0 & \mathbf{e}_4/2 & \mathbf{e}_7 \\ 0 & \mathbf{e}_2 & \mathbf{e}_8/2 & 0 & 0 & 0 \\ 0 & 0 & 0 & \mathbf{e}_5 & \mathbf{e}_8/2 & 0 \\ 0 & 0 & \mathbf{e}_2/2 & 0 & \mathbf{e}_5/2 & \mathbf{e}_8 \\ 0 & \mathbf{e}_3 & \mathbf{e}_9/2 & 0 & 0 & 0 \\ 0 & 0 & 0 & \mathbf{e}_6 & \mathbf{e}_9/2 & 0 \\ 0 & 0 & \mathbf{e}_3/2 & 0 & \mathbf{e}_6/2 & \mathbf{e}_9 \\ \mathbf{t}_1 & 0 & \mathbf{t}_3/2 & -\mathbf{t}_1 & 0 & -\mathbf{t}_1 \\ \mathbf{t}_2 & -\mathbf{t}_2 & 0 & 0 & \mathbf{t}_3/2 & -\mathbf{t}_2 \\ \mathbf{t}_3 & -\mathbf{t}_3 & \mathbf{t}_1/2 & -\mathbf{t}_3 & \mathbf{t}_2/2 & 0 \end{pmatrix} \quad (32)$$

APPENDIX B

EXPRESSION OF THE COST FUNCTION BASED ON THE EPIPOLAR ERROR IN TERMS OF THE ROTATION AND TRANSLATION COMPONENTS OF THE ESSENTIAL MATRIX

In this Section we will first develop the explicit expressions for the matrices  $\mathbf{M}_t$  and  $\mathbf{M}_R$ , showing that the objective functions in Theorem (V.1) are all equivalent. Then, the relation between these and the previous works [11] and [27] are explicitly derived. We want to point out that the equivalence between the cost functions was first given by Briales *et al.* in [27] by manipulating the algebraic error employed in each optimization problem.

Let us first recall the chain of equalities given in (V.1):

$$\frac{1}{2} \mathbf{e}^T \mathbf{C} \mathbf{e} = \frac{1}{2} \mathbf{t}^T \mathbf{M}_t \mathbf{t} = \quad (33)$$

$$= \frac{1}{2} \mathbf{r}^T \mathbf{M}_R \mathbf{r} \quad (34)$$

and the expression given for the coefficient matrix  $\mathbf{C}$

$$\mathbf{C} = \sum_{i=1}^N (\mathbf{f}'_i \otimes \mathbf{f}_i)(\mathbf{f}'_i \otimes \mathbf{f}_i)^T. \quad (35)$$

Consider the definition of the essential matrix in (2) and the identity:

$$\mathbf{Y} = \mathbf{C} \mathbf{X} \mathbf{B}^T \Leftrightarrow \text{vec}(\mathbf{Y}) = (\mathbf{B} \otimes \mathbf{C}) \text{vec}(\mathbf{X}), \quad (36)$$

where all the matrices are of compatible dimension. We can now express  $\mathbf{E} = [\mathbf{t}]_{\times} \mathbf{R}$  in two different useful forms:

$$\text{vec}(\mathbf{E}) = (\mathbf{I}_3 \otimes [\mathbf{t}]_{\times}) \text{vec}(\mathbf{R}) \quad (37)$$

$$\text{vec}(\mathbf{E}) = (\mathbf{R}^T \otimes \mathbf{I}_3) \text{vec}([\mathbf{t}]_{\times}) \quad (38)$$

A. *Objective cost as a function of the translation component.*

Let us define the matrix  $\mathbf{B} \in \mathbb{R}^{9 \times 3}$  such that:

$$\text{vec}([\mathbf{t}]_{\times}) = \mathbf{B} \mathbf{t}. \quad (39)$$

We can now introduce (38) and (39) into the original cost function:

$$\text{vec}([\mathbf{t}]_{\times})^T (\mathbf{R}^T \otimes \mathbf{I}_3)^T \mathbf{C} (\mathbf{R}^T \otimes \mathbf{I}_3) \text{vec}([\mathbf{t}]_{\times}) = \quad (40)$$

$$= \mathbf{t}^T \mathbf{B}^T (\mathbf{R}^T \otimes \mathbf{I}_3)^T \underbrace{\mathbf{C} (\mathbf{R}^T \otimes \mathbf{I}_3) \mathbf{B}}_{\tilde{\mathbf{R}}} \mathbf{t} = \mathbf{t}^T \underbrace{\tilde{\mathbf{R}}^T \mathbf{C} \tilde{\mathbf{R}}}_{\mathbf{M}_t} \mathbf{t}, \quad (41)$$

where  $\tilde{\mathbf{R}}^T = -[[\mathbf{r}_1]_{\times}, [\mathbf{r}_2]_{\times}, [\mathbf{r}_3]_{\times}]^T \in \mathbb{R}^{9 \times 3}$  with  $\{\mathbf{r}_i\}_{i=1}^3$  the columns of  $\mathbf{R}$  and  $\mathbf{M}_t \in \mathbb{S}^3$  by construction. The objective function  $\frac{1}{2} \mathbf{t}^T \mathbf{M}_t \mathbf{t}$  is quadratic in  $\mathbf{R}$  and  $\mathbf{t}$  and allows us to derive the gradient and Hessian w.r.t.  $\mathbf{t}$  in a simpler way.

**Relation with the objective function in [11]:**

Some algebraic manipulation in (40) yields the same objective function employed by Kneip and Lynen in [11], as follows:

$$\text{vec}([\mathbf{t}]_{\times})^T (\mathbf{R}^T \otimes \mathbf{I}_3)^T \mathbf{C} (\mathbf{R}^T \otimes \mathbf{I}_3) \text{vec}([\mathbf{t}]_{\times}) = \quad (42)$$

$$\text{vec}([\mathbf{t}]_{\times})^T (\mathbf{R}^T \otimes \mathbf{I}_3)^T \left( \sum_{i=1}^N (\mathbf{f}'_i \otimes \mathbf{f}_i) (\mathbf{f}'_i \otimes \mathbf{f}_i)^T \right) (\mathbf{R}^T \otimes \mathbf{I}_3) \text{vec}([\mathbf{t}]_{\times}) = \quad (43)$$

$$\stackrel{(1)}{=} \sum_{i=1}^N (\text{vec}([\mathbf{t}]_{\times})^T (\mathbf{R} \otimes \mathbf{I}_3) (\mathbf{f}'_i \otimes \mathbf{f}_i) (\mathbf{f}'_i \otimes \mathbf{f}_i)^T (\mathbf{R} \otimes \mathbf{I}_3)^T \text{vec}([\mathbf{t}]_{\times})) = \quad (44)$$

$$\stackrel{(2)}{=} \sum_{i=1}^N (\text{vec}([\mathbf{t}]_{\times})^T (\mathbf{R} \mathbf{f}'_i \otimes \mathbf{f}_i) (\mathbf{R} \mathbf{f}'_i \otimes \mathbf{f}_i)^T \text{vec}([\mathbf{t}]_{\times})) = \quad (45)$$

$$\stackrel{(3)}{=} \sum_{i=1}^N (\mathbf{f}_i^T [\mathbf{t}]_{\times} (\mathbf{R} \mathbf{f}'_i))^T (\mathbf{f}_i^T [\mathbf{t}]_{\times} (\mathbf{R} \mathbf{f}'_i)) = \quad (46)$$

$$\stackrel{(4)}{=} \sum_{i=1}^N (\mathbf{f}_i^T \mathbf{R} \mathbf{f}'_i{}^T \mathbf{t})^T (\mathbf{f}_i^T \text{vec}([\mathbf{R} \mathbf{f}'_i]_{\times})^T \mathbf{t}) = \quad (47)$$

$$\stackrel{(5)}{=} \sum_{i=1}^N (\text{vec}([\mathbf{R} \mathbf{f}'_i]_{\times}) \mathbf{f}_i^T \mathbf{t})^T (\text{vec}([\mathbf{R} \mathbf{f}'_i]_{\times}) \mathbf{f}_i^T \mathbf{t}) = \quad (48)$$

$$\stackrel{(6)}{=} \sum_{i=1}^N ((\mathbf{f}_i \times \mathbf{R} \mathbf{f}'_i)^T \mathbf{t})^T ((\mathbf{f}_i \times \mathbf{R} \mathbf{f}'_i)^T \mathbf{t}) = \quad (49)$$

$$\stackrel{(7)}{=} \mathbf{t}^T \underbrace{\left( \sum_{i=1}^N (\mathbf{f}_i \times \mathbf{R} \mathbf{f}'_i) (\mathbf{f}_i \times \mathbf{R} \mathbf{f}'_i)^T \right)}_{\mathbf{M}_t} \mathbf{t}, \quad (50)$$

which is the objective function to be minimized in [11].

The performed steps are:

- 1) Introduce the definition of  $\mathbf{C}$  given in (35).
- 2) "Move" the constant terms inside the sum over  $i$ .
- 3) Apply the identity:  $(\mathbf{A} \otimes \mathbf{B})(\mathbf{C} \otimes \mathbf{D}) = (\mathbf{A}\mathbf{C} \otimes \mathbf{B}\mathbf{D})$ .
- 4) Use the expression in (36) to obtain a single term.
- 5) Consider that  $\mathbf{B}^t \mathbf{A}^t = (\mathbf{A}\mathbf{B})^t$ .
- 6) Apply the anticommutative property of the cross product, *i.e.*  $\mathbf{a} \times \mathbf{b} = -\mathbf{b} \times \mathbf{a}$ .
- 7) Develop the transposed parenthesis and "move" outside the sum over  $i$  the constant term  $\mathbf{t}$ .

### B. Objective function as a function of the rotation component.

Similarly, we first develop the form for  $M_R$  and then relate our results with those described by Briaies *et al.* in [27]. We introduce (37) in our original cost function and use  $\mathbf{R} = \text{vec}(\mathbf{R})$ . The matrix  $M_R$  is obtained as

$$\mathbf{r}^T (\mathbf{I}_3 \otimes [\mathbf{t}]_{\times})^T \underbrace{\mathbf{C}}_{\tilde{\mathbf{T}}} (\mathbf{I}_3 \otimes [\mathbf{t}]_{\times}) \mathbf{r} = \mathbf{r}^T \underbrace{\tilde{\mathbf{T}}^T \mathbf{C} \tilde{\mathbf{T}}}_{M_R} \mathbf{r}. \quad (51)$$

Similarly, the cost function defined by  $M_R$  is quadratic in the entries of  $\mathbf{R}$ ,  $\mathbf{t}$  and yields a simple expression for the computation of the gradient and Hessian w.r.t.  $\mathbf{R}$ .

#### Relation with the objective function in [27]:

Let us introduce the definition of  $\mathbf{C}$  in (51) and manipulate the expression as follows:

$$\mathbf{r}^T (\mathbf{I}_3 \otimes [\mathbf{t}]_{\times})^T \left( \sum_{i=1}^N (\mathbf{f}'_i \otimes \mathbf{f}_i) (\mathbf{f}'_i \otimes \mathbf{f}_i)^T \right) (\mathbf{I}_3 \otimes [\mathbf{t}]_{\times}) \mathbf{r} = \quad (52)$$

$$\stackrel{(1)}{=} \mathbf{r}^T \left( \sum_{i=1}^N (\mathbf{I}_3 \otimes [\mathbf{t}]_{\times})^T (\mathbf{f}'_i \otimes \mathbf{f}_i) (\mathbf{f}'_i \otimes \mathbf{f}_i)^T (\mathbf{I}_3 \otimes [\mathbf{t}]_{\times}) \right) \mathbf{r} = \quad (53)$$

$$\stackrel{(2)}{=} \mathbf{r}^T \left( \sum_{i=1}^N (\mathbf{f}'_i \otimes [\mathbf{t}]_{\times}^T \mathbf{f}_i) (\mathbf{f}'_i \otimes [\mathbf{t}]_{\times}^T \mathbf{f}_i)^T \right) \mathbf{r} = \quad (54)$$

$$\stackrel{(3)}{=} \mathbf{r}^T \underbrace{\left( \sum_{i=1}^N (\mathbf{f}'_i \otimes [\mathbf{f}_i]_{\times} \mathbf{t}) (\mathbf{f}'_i \otimes [\mathbf{f}_i]_{\times} \mathbf{t})^T \right)}_{M_R} \mathbf{r} = \quad (55)$$

$$\stackrel{(4)}{=} \mathbf{r}^T \sum_{i=1}^N \left( (\mathbf{f}'_i \otimes [\mathbf{f}_i]_{\times} \sum_{j,k=1}^3 (t_j \mathbf{e}_j)) (\mathbf{f}'_i \otimes [\mathbf{f}_i]_{\times} \sum_{j,k=1}^3 (t_k \mathbf{e}_k))^T \right) \mathbf{r} = \quad (56)$$

$$\stackrel{(5)}{=} \mathbf{r}^T \sum_{i=1}^N \left( (\mathbf{f}'_i \otimes \sum_{j=1}^3 ([\mathbf{f}_i]_{\times} t_j \mathbf{e}_j)) (\mathbf{f}'_i \otimes \sum_{k=1}^3 ([\mathbf{f}_i]_{\times} t_k \mathbf{e}_k))^T \right) \mathbf{r} = \quad (57)$$

$$\stackrel{(6)}{=} \mathbf{r}^T \sum_{i=1}^N \left( \sum_{j,k=1}^3 ((\mathbf{f}'_i \otimes [\mathbf{f}_i]_{\times} t_j \mathbf{e}_j) (\mathbf{f}'_i \otimes [\mathbf{f}_i]_{\times} t_k \mathbf{e}_k)^T) \right) \mathbf{r} = \quad (58)$$

$$\stackrel{(7)}{=} t_j \mathbf{r}^T \underbrace{\left( \sum_{i=1}^N (\mathbf{f}'_i \otimes (\mathbf{f}_i \times \mathbf{e}_j)) (\mathbf{f}'_i \otimes (\mathbf{f}_i \times \mathbf{e}_k))^T \right)}_{C_{jk}} \mathbf{r} t_k, \quad (59)$$

which is the cost function employed in [27].

The main performed step are:

- 1) "Move" the constant terms in  $\mathbf{t}$  inside the sum over  $i$ .
- 2) Apply the relation  $(\mathbf{A} \otimes \mathbf{B})(\mathbf{C} \otimes \mathbf{D}) = (\mathbf{AC} \otimes \mathbf{BD})$ .
- 3) Use the anticommutative property of the cross product.
- 4) The cross product with a 3D vector can be expressed as a matrix multiplication, *i.e.*, it's linear:  $[\mathbf{a}]_{\times} \mathbf{b} = [\mathbf{a}]_{\times} b_1 \mathbf{e}_1 + [\mathbf{a}]_{\times} b_2 \mathbf{e}_2 + [\mathbf{a}]_{\times} b_3 \mathbf{e}_3$ , where  $\mathbf{e}_i$  denotes the canonical vector in  $\mathbb{R}^3$ .
- 5) Apply the associative property of the kronecker product, *i.e.*  $\mathbf{a} \otimes (\mathbf{b} + \dots \mathbf{C}) = \mathbf{a} \otimes \mathbf{b} + \dots + \mathbf{a} \otimes \mathbf{C}$ .
- 6) "Move" the constant, scalar terms  $t_j, t_k$  outside the sums. Finally, swap the order of the sums.

## APPENDIX C

### TERMS OF THE QUADRATIC MODEL FOR THE COST FUNCTION IN TERMS OF THE ROTATION AND TRANSLATION

In this Section we derive the Euclidean gradient and Hessian of the cost function considered in this work w.r.t. the points on the manifold  $\text{SO}(3) \times S^2$ .

Since the considered manifold is a direct product, its tangent bundle  $TM$  [42] is expressed as:  $TM = T_R \times T_t$ , where  $T_R$  and  $T_t$  are the tangent bundles of  $\text{SO}(3)$  and  $S^2$ , respectively [16]. This implies that we can write any vector field  $\dot{Y}$  as the composition of its components in the two subspaces  $T_R, T_t$  *i.e.*,  $\dot{Y} = (\dot{Y}_{\text{SO}(3)}, \dot{Y}_{S^2}) \in T_R \times T_t$ , which simplifies the derivation of them.

#### Gradient:

Considering the cost function as a function restricted to the embedded manifold [42], the relation between the Euclidean gradient and its Riemannian counterpart is simplify to:

$$\text{grad}f(\mathbf{R}, \mathbf{t}) = (\text{Proj}_{\mathbf{R}}(\nabla_{\mathbf{R}}f(\mathbf{R}, \mathbf{t})), \text{Proj}_{\mathbf{t}}(\nabla_{\mathbf{t}}f(\mathbf{R}, \mathbf{t}))), \quad (60)$$

where  $\text{Proj}_{\mathbf{R}}(\bullet)$  and  $\text{Proj}_{\mathbf{t}}(\bullet)$  denote the orthogonal projection operator onto the tangent spaces of  $\text{SO}(3)$  and  $\mathcal{S}^2$  at the points  $\mathbf{R}, \mathbf{t}$ , respectively [42]:

$$\text{Proj}_{\mathbf{R}} : \mathbb{T}_{\mathbf{R}}(\mathbb{R}^{3 \times 3}) \longrightarrow \mathbb{T}_{\mathbf{R}}(\text{SO}(3)) \quad (61)$$

$$\text{Proj}_{\mathbf{R}}(\mathbf{X}) = \mathbf{R}\text{skew}(\mathbf{R}^T \mathbf{X}), \quad (62)$$

where  $\text{skew}(\mathbf{A})$  extracts the skew-symmetric part of the matrix  $\mathbf{A}$ , *i.e.*  $\text{skew}(\mathbf{A}) = \frac{1}{2}(\mathbf{A} - \mathbf{A}^T)$  and

$$\text{Proj}_{\mathbf{t}} : \mathbb{T}_{\mathbf{t}}(\mathbb{R}^3) \longrightarrow \mathbb{T}_{\mathbf{t}}(\mathcal{S}^2) \quad (63)$$

$$\text{Proj}_{\mathbf{t}}(\mathbf{x}) = \mathbf{x} - (\mathbf{t}^T \mathbf{x})\mathbf{t} \quad (64)$$

The Euclidean gradient  $\nabla f(\mathbf{R}, \mathbf{t}) = (\nabla_{\mathbf{R}}f(\mathbf{R}, \mathbf{t}), \nabla_{\mathbf{t}}f(\mathbf{R}, \mathbf{t}))$  reads:

$$\nabla_{\mathbf{R}}f(\mathbf{R}, \mathbf{t}) = \mathbf{M}_{\mathbf{R}} \mathbf{r} \quad \nabla_{\mathbf{t}}f(\mathbf{R}, \mathbf{t}) = \mathbf{M}_{\mathbf{t}} \mathbf{t}. \quad (65)$$

### Hessian-vector product:

Similarly, the Hessian counterparts are derived by considering the embedded manifold:

$$\text{Hess}_{\mathbf{R}}(\mathbf{R}, \mathbf{t})[\dot{\mathbf{R}}, \dot{\mathbf{t}}] = \text{Proj}_{\mathbf{R}}\left(\nabla_{\mathbf{R}}^2 f(\mathbf{R}, \mathbf{t})[\dot{\mathbf{R}}, \dot{\mathbf{t}}] - \dot{\mathbf{R}}^T \text{sym}(\mathbf{R} \nabla_{\mathbf{R}}f(\mathbf{R}, \mathbf{t}))\right) \quad (66)$$

$$\text{Hess}_{\mathbf{t}}(\mathbf{R}, \mathbf{t})[\dot{\mathbf{R}}, \dot{\mathbf{t}}] = \text{Proj}_{\mathbf{t}}\left(\nabla_{\mathbf{t}}^2 f(\mathbf{R}, \mathbf{t})[\dot{\mathbf{R}}, \dot{\mathbf{t}}] - (\mathbf{t}^T \nabla_{\mathbf{t}}f(\mathbf{R}, \mathbf{t}))\dot{\mathbf{t}}\right), \quad (67)$$

where  $\text{sym}(\mathbf{A})$  extracts the symmetric part of the matrix  $\mathbf{A}$  *i.e.*,  $\text{sym}(\mathbf{A}) = \frac{1}{2}(\mathbf{A} + \mathbf{A}^T)$ .

The action of the Euclidean Hessian on the vector  $(\dot{\mathbf{R}}, \dot{\mathbf{t}})$  is calculated by applying multivariate calculus as

$$\nabla^2 f(\mathbf{R}, \mathbf{t})[\dot{\mathbf{R}}, \dot{\mathbf{t}}] = (\nabla_{\mathbf{R}}^2 f(\mathbf{R}, \mathbf{t})[\dot{\mathbf{R}}, \dot{\mathbf{t}}], \nabla_{\mathbf{t}}^2 f(\mathbf{R}, \mathbf{t})[\dot{\mathbf{R}}, \dot{\mathbf{t}}]). \quad (68)$$

The component for the rotation is computed as:

$$\nabla_{\mathbf{R}}^2 f(\mathbf{R}, \mathbf{t})[\dot{\mathbf{R}}, \dot{\mathbf{t}}] = \nabla_{\mathbf{R}\mathbf{R}}f(\mathbf{R}, \mathbf{t})[\dot{\mathbf{R}}] + \nabla_{\mathbf{R}\mathbf{t}}f(\mathbf{R}, \mathbf{t})[\dot{\mathbf{t}}] \quad (69)$$

$$\nabla_{\mathbf{R}\mathbf{R}}f(\mathbf{R}, \mathbf{t})[\dot{\mathbf{R}}] = \mathbf{M}_{\mathbf{R}} \dot{\mathbf{r}} \quad (70)$$

$$\nabla_{\mathbf{R}\mathbf{t}}f(\mathbf{R}, \mathbf{t})[\dot{\mathbf{t}}] = \mathbf{M}_{\mathbf{t}, \mathbf{R}} \dot{\mathbf{t}}, \quad (71)$$

where  $\mathbf{M}_{\mathbf{t}, \mathbf{R}}(\mathbf{R}, \mathbf{t}) \doteq \mathbf{M}_{\mathbf{t}, \mathbf{R}}(\mathbf{R}, \mathbf{t})$  will be defined later.

The component for the translation is:

$$\nabla_{\mathbf{t}}^2 f(\mathbf{R}, \mathbf{t})[\dot{\mathbf{R}}, \dot{\mathbf{t}}] = \nabla_{\mathbf{t}\mathbf{t}}f(\mathbf{R}, \mathbf{t})[\dot{\mathbf{t}}] + \nabla_{\mathbf{t}\mathbf{R}}f(\mathbf{R}, \mathbf{t})[\dot{\mathbf{R}}] \quad (72)$$

$$\nabla_{\mathbf{t}\mathbf{t}}f(\mathbf{R}, \mathbf{t})[\dot{\mathbf{t}}] = \mathbf{M}_{\mathbf{t}} \dot{\mathbf{t}} \quad (73)$$

$$\nabla_{\mathbf{t}\mathbf{R}}f(\mathbf{R}, \mathbf{t})[\dot{\mathbf{t}}] = \mathbf{M}_{\mathbf{R}, \mathbf{t}} \dot{\mathbf{R}}, \quad (74)$$

with  $\mathbf{M}_{\mathbf{R}, \mathbf{t}} \doteq \mathbf{M}_{\mathbf{R}, \mathbf{t}}(\mathbf{R}, \mathbf{t})$  and  $\mathbf{M}_{\mathbf{R}, \mathbf{t}}(\mathbf{R}, \mathbf{t}) = \mathbf{M}_{\mathbf{t}, \mathbf{R}}(\mathbf{R}, \mathbf{t})^T$  by symmetry of the Hessian.

### Derivation of $\mathbf{M}_{\mathbf{R}, \mathbf{t}}(\mathbf{R}, \mathbf{t})$

See that

$$\mathbf{M}_{\mathbf{R}, \mathbf{t}} = \frac{\partial(\partial f(\mathbf{R}, \mathbf{t}))}{\partial \mathbf{r} \partial \mathbf{t}} = \frac{\partial(\mathbf{M}_{\mathbf{t}} \mathbf{t})}{\partial \mathbf{r}} \in \mathbb{R}^{3 \times 9}, \quad (75)$$

and

$$\mathbf{M}_{\mathbf{t}} \mathbf{t} = \tilde{\mathbf{R}}^T \mathbf{C} \tilde{\mathbf{R}} \mathbf{t} = \tilde{\mathbf{R}}^T \mathbf{C} \tilde{\mathbf{T}} \mathbf{r} \in \mathbb{R}^3, \quad (76)$$

where we have used the definition of  $\mathbf{e}$  given in (38) for the second equality (in the first one we substituted the definition of  $\mathbf{M}_{\mathbf{t}}$  in []).

Recall that  $\tilde{\mathbf{R}}^T \in \mathbb{R}^{3 \times 9}$  and let  $\tilde{\mathbf{r}}_i \in \mathbb{R}^{1 \times 9}$  be the  $i$ -th row of the matrix, *i.e.*,

$$\tilde{\mathbf{R}}^T = \begin{pmatrix} \tilde{\mathbf{r}}_1 \\ \tilde{\mathbf{r}}_2 \\ \tilde{\mathbf{r}}_3 \end{pmatrix} \quad (77)$$

See that we can express each row as  $\tilde{r}_i = r^T B_i$ , where  $B_i \in \mathbb{R}^{9 \times 9}$  are sparse matrices (shown in Equation (81)). Then, the  $i$ -th row of  $M_{t.R}$  is given by

$$\tilde{r}_i C \tilde{T} r = r^T B_i C \tilde{T} r, \quad (78)$$

and its derivate w.r.t.  $r$  is  $2B_i C \tilde{T} r \in \mathbb{R}^{9 \times 1}$ . The gradient  $M_{R.t}$  is obtained by stacking the derivative of each row.

A similar procedure can be given for  $M_{t.R} \in \mathbb{R}^{9 \times 3}$ , by defining a set of matrices  $A_i \in \mathbb{R}^{3 \times 9}$ ,  $i = 1, \dots, 9$  such that the  $i$ -th row of  $\tilde{T} \in \mathbb{R}^{9 \times 9}$ ,  $\tilde{t}_1 \in \mathbb{R}^{1 \times 9}$  can be expressed as  $\tilde{t}_1 = t^T A_i$ .

Then,

$$M_{t.R} = \frac{\partial(M_{Rr})}{\partial t}, \quad (79)$$

with

$$M_{Rr} = \tilde{T}^T C \tilde{T} r = \tilde{T}^T C \tilde{R} t. \quad (80)$$

Its  $i$ -th row is given by  $t^T A_i C \tilde{R} t$  and its derivative w.r.t.  $t$  by  $2A_i C \tilde{R} t \in \mathbb{R}^3$ . Again,  $M_{t.R}$  is obtained by stacking all the derivatives (nine in total) of the rows. We do not include the explicit expressions for  $A_i$  given their similarity with  $B_i$  (Equation (81)).

Although it may not seem apparent, the expression of  $M_{R.t}$ ,  $M_{t.R}$  given above fulfills the relation  $M_{t.R} = M_{R.t}^T$ .

$$B_1 = \begin{pmatrix} 0 & 0 & 0 & 0 & 0 & 0 & 0 & 0 & 0 \\ 0 & 0 & -1 & 0 & 0 & 0 & 0 & 0 & 0 \\ 0 & 1 & 0 & 0 & 0 & 0 & 0 & 0 & 0 \\ 0 & 0 & 0 & 0 & 0 & 0 & 0 & 0 & 0 \\ 0 & 0 & 0 & 0 & 0 & -1 & 0 & 0 & 0 \\ 0 & 0 & 0 & 0 & 1 & 0 & 0 & 0 & 0 \\ 0 & 0 & 0 & 0 & 0 & 0 & 0 & 0 & 0 \\ 0 & 0 & 0 & 0 & 0 & 0 & 0 & 0 & -1 \\ 0 & 0 & 0 & 0 & 0 & 0 & 0 & 1 & 0 \end{pmatrix}, B_2 = \begin{pmatrix} 0 & 0 & 1 & 0 & 0 & 0 & 0 & 0 & 0 \\ 0 & 0 & 0 & 0 & 0 & 0 & 0 & 0 & 0 \\ -1 & 0 & 0 & 0 & 0 & 0 & 0 & 0 & 0 \\ 0 & 0 & 0 & 0 & 0 & 1 & 0 & 0 & 0 \\ 0 & 0 & 0 & 0 & 0 & 0 & 0 & 0 & 0 \\ 0 & 0 & 0 & -1 & 0 & 0 & 0 & 0 & 0 \\ 0 & 0 & 0 & 0 & 0 & 0 & 0 & 0 & 1 \\ 0 & 0 & 0 & 0 & 0 & 0 & 0 & 0 & 0 \\ 0 & 0 & 0 & 0 & 0 & 0 & -1 & 0 & 0 \end{pmatrix}, B_3 = \begin{pmatrix} 0 & -1 & 0 & 0 & 0 & 0 & 0 & 0 & 0 \\ 1 & 0 & 0 & 0 & 0 & 0 & 0 & 0 & 0 \\ 0 & 0 & 0 & 0 & 0 & 0 & 0 & 0 & 0 \\ 0 & 0 & 0 & 0 & -1 & 0 & 0 & 0 & 0 \\ 0 & 0 & 0 & 1 & 0 & 0 & 0 & 0 & 0 \\ 0 & 0 & 0 & 0 & 0 & 0 & 0 & 0 & 0 \\ 0 & 0 & 0 & 0 & 0 & 0 & 0 & -1 & 0 \\ 0 & 0 & 0 & 0 & 0 & 0 & 1 & 0 & 0 \\ 0 & 0 & 0 & 0 & 0 & 0 & 0 & 0 & 0 \end{pmatrix} \quad (81)$$

#### APPENDIX D

##### EXPERIMENTS ON REAL DATA: DATASETS

The experiments in Section (VII-C) were performed in the following sequences:

- **ETH3D**: playground; relief; botanical\_garden; boulders; exhibition\_hall; living\_room; observatory; terrace; terrace\_2; terrains; statue.
- **CVPR08**: Herz-Jesu-P8; castle-P19; castle-P30; fountain-P11; Herz-Jesu-P25; entry-P10; .
- **TUM**: rgb\_d\_dataset\_freiburg3\_long\_office\_household; rgb\_d\_dataset\_freiburg3\_structure\_texture\_far; rgb\_d\_dataset\_freiburg3\_structure\_texture\_near; rgb\_d\_dataset\_freiburg3\_large\_cabinet.

#### APPENDIX E

##### EXPERIMENTS ON REAL DATA: RESULTS

In this Section we break down the general statistics reported in the main document. Concretely, we show for each sequence of each dataset (ETH3D, TUM, CVPR08) the error in rotation measured in terms of geodesic distance w.r.t. the ground-truth and list the percentage of cases in which our verification in Algorithm (1) could certify the optimality of the solution.

- **ETH3D**: playground (100%); relief (92%); botanical\_garden (100%); boulders (100%); exhibition\_hall (94%); living\_room (97.9167%); observatory (100%); terrace (100%); terrace\_2 (100%); terrains (100%); statue (100%).
- **CVPR08**: Herz-Jesu-P8 (100%); castle-P19 (94.44%); castle-P30 (100%); fountain-P11 (100%); Herz-Jesu-P25 (100%); entry-P10 (100%); .
- **TUM**: rgb\_d\_dataset\_freiburg3\_long\_office\_household (98.7179%); rgb\_d\_dataset\_freiburg3\_structure\_texture\_far (75.8065%); rgb\_d\_dataset\_freiburg3\_structure\_texture\_near (74.1379%); rgb\_d\_dataset\_freiburg3\_large\_cabinet (81.8182%).

Figure (13), (15) and (17) depicts the error in rotation for the proposed robust pipeline in ALgorithm (2) (OURS), the error for those cases with certifier optimal solution (OURS-CERT), and the minimal solvers (5-PT, 7-PT and 8-PT) embedded into RANSAC paradigms (RANSAC-5PT, RANSAC-7PT and RANSAC-8PT, respectively)

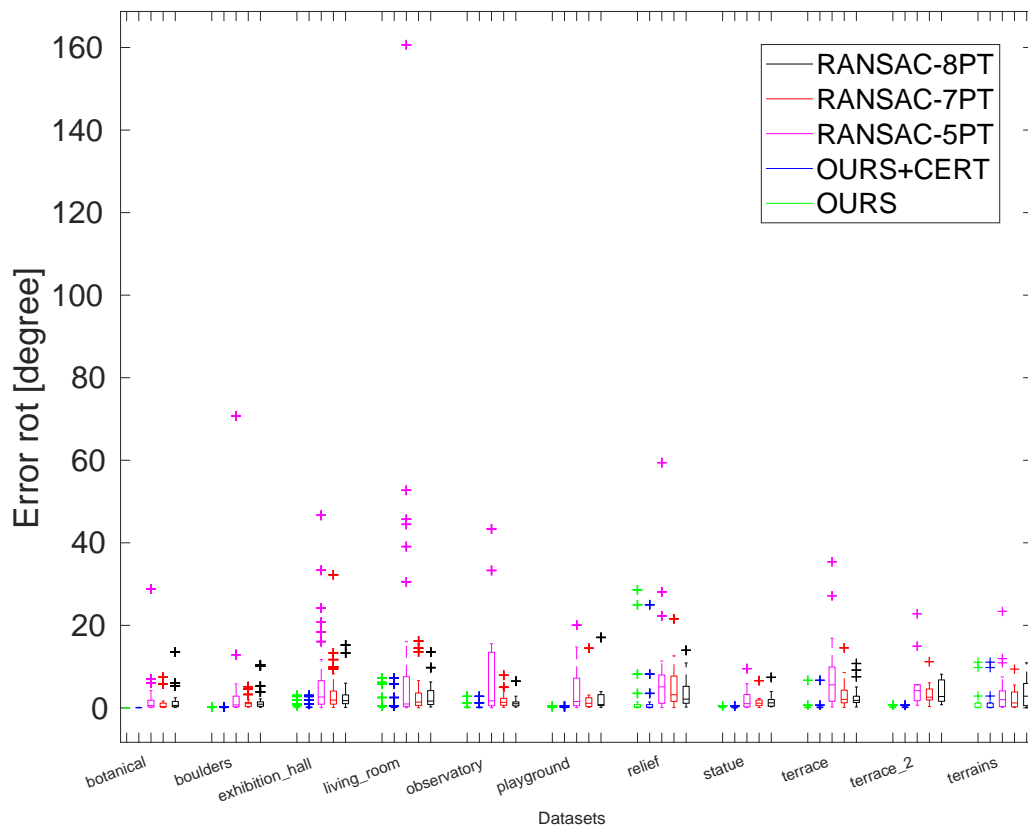


Fig. 13

Fig. 14: Error in rotation w.r.t. the ground-truth for the different sequences of the ETH3D dataset.

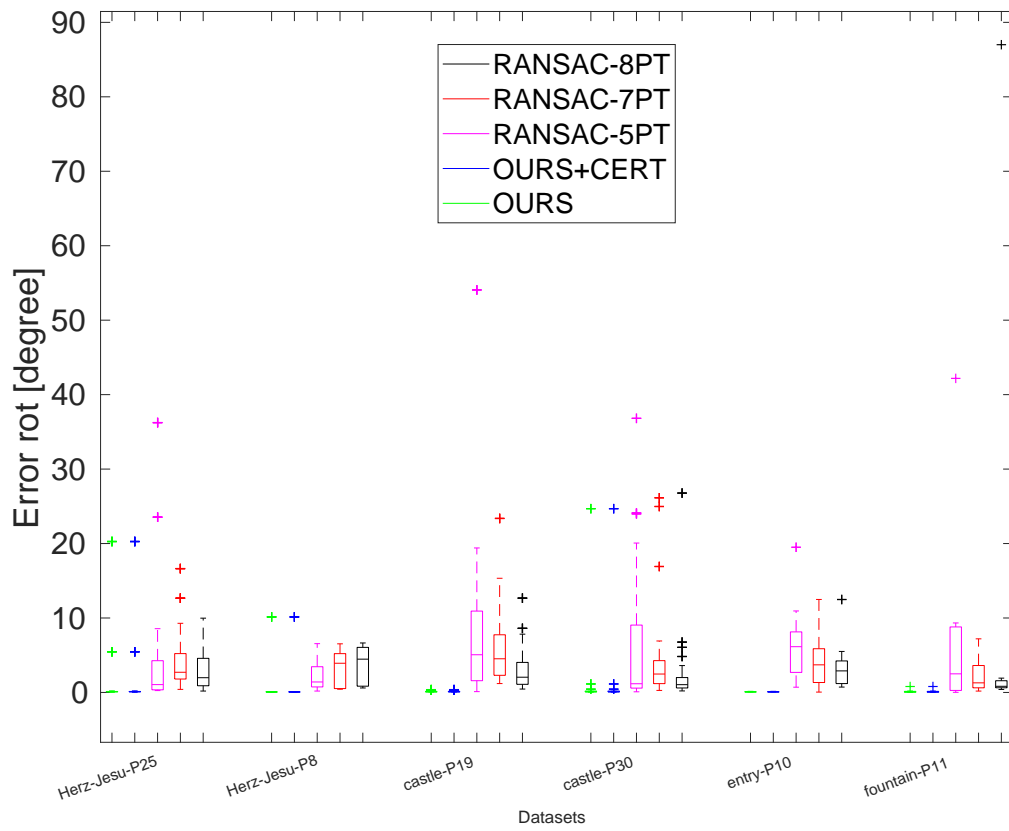


Fig. 15

Fig. 16: Error in rotation w.r.t. the ground-truth for the different sequences of the CVPR08 dataset.

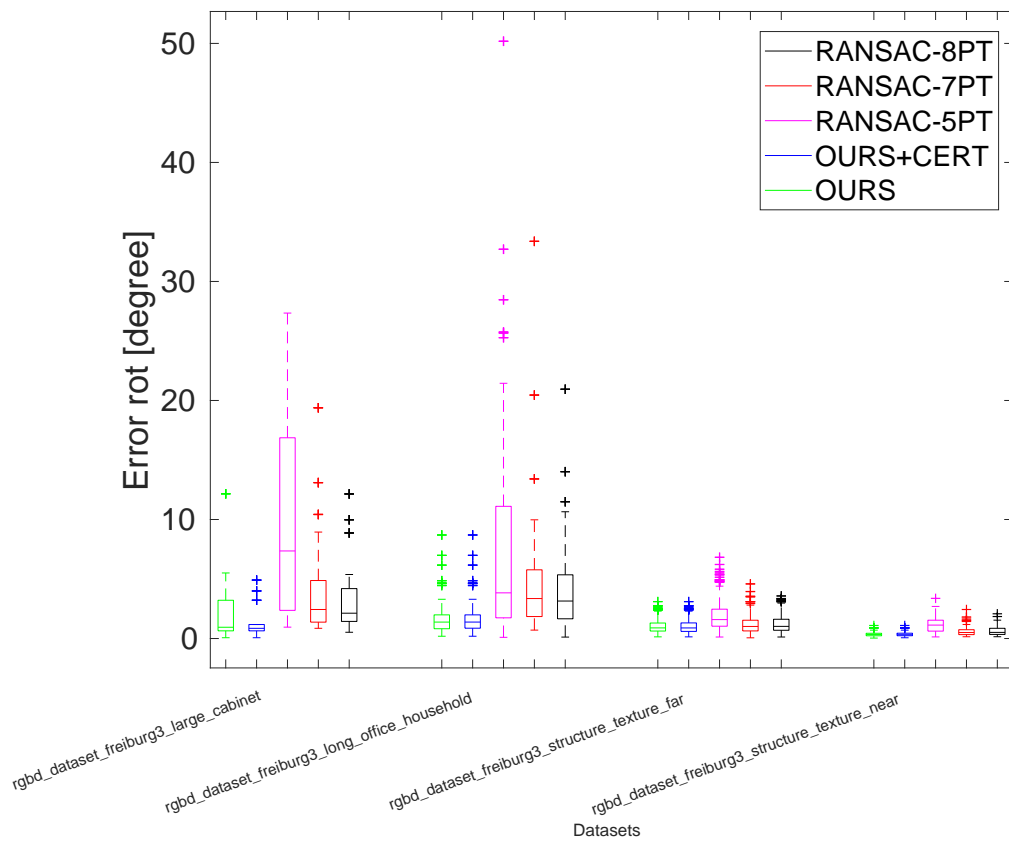


Fig. 17

Fig. 18: Error in rotation w.r.t. the ground-truth for the different sequences of the TUM dataset.